Iranian Journal of Basic Medical Sciences
ijbms.mums.ac.ir

Controlled stepwise serum deprivation enhances physicochemical properties and biocompatibility of small extracellular vesicle-enriched particles derived from adipose mesenchymal stem cells

Pegah Rajabi [1#], Nazanin Akbari [2#], Hanieh Jafary [1], Banafsheh Heidari [3*]

[1] Department of Biology, Science and Research Branch, Islamic Azad University, Tehran, Iran
[2] Department of Biology, Shahid Beheshti University, Tehran, Iran
[3] Department of Photo Healing and Regeneration, Medical Laser Research Center, Yara Institute, ACECR, Tehran, Iran

ARTICLE INFO

Article type:
Original

Article history:
Received: Aug 2, 2026
Accepted: Sep 27, 2026

Keywords:
Cell movement
Culture media
Extracellular vesicles
Mesenchymal stem cells
Particle size
Regenerative medicine
Serum-free
Toxicity tests

ABSTRACT

Objective(s): This study assessed how controlled, sequential serum deprivation affects adipose-derived mesenchymal stromal cells (AdMSCs) and the physicochemical properties and biocompatibility of their extracellular vesicle-enriched particles.

Materials and Methods: AdMSCs from five healthy donors were cultured under stepwise serum deprivation (from 10% exosome-depleted FBS to 5%, then 1%) and standard control conditions (10% exosome-depleted FBS) for 36 hr. The effects of these culture conditions on AdMSC density, apoptosis, migration, and stemness were assessed. AdMSC-derived sEV-enriched particles were isolated and characterized for morphological, biochemical, and structural features using field emission scanning electron microscopy (FESEM), TEM, FTIR, DLS, Zeta potential, and Bradford assays, performed in triplicate. Biocompatibility was evaluated using MTT, and *in vivo* irritation, sensitization, and acute systemic toxicity tests were conducted.

Results: No significant differences were observed in AdMSC cell number, viability, apoptosis, or stemness; however, stepwise serum starvation significantly enhanced migration. FESEM and TEM analyses revealed improved quality, greater structural uniformity, and significantly reduced aggregation in serum-starved sEV-enriched particles. Starved particles showed a distinct dry-size peak of 47±15 to 49±13 nm, whereas controls had a broader average of 340±14 to 350±12 nm. Controls were polydisperse (80% at 227.7±45.7nm, 20% at 50.8±5.7nm), whereas starved particles were monodisperse (34.1±3.1nm). Starved particles exhibited higher zeta potential (-4.9 mV vs -9.0 mV) and protein content (4.3 vs 2.18 mg/ml; $P \leq 0.05$). Both groups showed acceptable biocompatibility, with no cytotoxicity, irritation, sensitization, or microbial contamination ($P > 0.05$).

Conclusion: Stepwise serum starvation significantly improved the morphological, biochemical, and structural properties of AdMSC-derived sEV-enriched particles without compromising their overall safety profile.

▶ Please cite this article as:
Rajabi P, Akbari N, Jafary H, Heidari B. Controlled stepwise serum deprivation enhances physicochemical properties and biocompatibility of small extracellular vesicle-enriched particles derived from adipose mesenchymal stem cells. Iran J Basic Med Sci 2027; 30:

Corrected Proof

Introduction

Although regenerative medicine has advanced significantly, the clinical translation of stem cell-based therapies remains constrained by several challenges, including immune incompatibility, the risk of ectopic tissue formation, tumorigenicity, vascular obstruction, and complex storage or transport requirements. These challenges have shifted scientific interest toward cell-free therapeutic strategies, particularly those involving small extracellular vesicles (sEVs), which may recapitulate the therapeutic benefits of their parent cells while offering greater safety, stability, and manufacturing scalability (1–3). sEVs, typically 30-150 nm in diameter, are lipid bilayer-enclosed nanoparticles secreted by almost all cell types. They serve as potent mediators of intercellular communication by transferring proteins, lipids, messenger RNAs, microRNAs, and other signaling molecules to recipient cells (4, 5). Because of their biological stability, low immunogenicity, minimal risk of embolic complications, and ability to penetrate biological barriers, sEVs have emerged as promising candidates for tissue repair, immunomodulation, targeted drug delivery, and biomarker discovery (6–9). Among available cellular sources, mesenchymal stem/stromal cells (MSCs) are widely investigated as a source of therapeutic sEVs because of their regenerative, anti-inflammatory, angiogenic, and immunoregulatory properties. Among the different MSC sources, adipose tissue-derived MSCs (AdMSCs) offer several practical advantages, including tissue accessibility, minimally invasive harvesting, high proliferative capacity, and efficient *in vitro* expansion, making them a practical, scalable, and versatile source for next-generation

*__Corresponding author:__ Banafsheh Heidari. Department of Photo Healing and Regeneration, Medical Laser Research Center, Yara Institute, ACECR, Tehran, Iran.
Email: ban_heidari@yahoo.com, b.heidari@acecr.ac.ir
#These authors contributed equally to this work

© 2027. This work is openly licensed via CC BY 4.0.
This is an Open Access article distributed under the terms of the Creative Commons Attribution License (https://creativecommons.org/licenses), which permits unrestricted use, distribution, and reproduction in any medium, provided the original work is properly cited.

vesicle-based therapeutics (10, 11). Furthermore, sEVs from AdMSCs (AdMSC-derived sEVs or AdMSC-derived sEV-enriched particles) have shown biological activities associated with angiogenesis, inflammation modulation, extracellular matrix remodeling, and wound repair (11–13). Successful clinical translation of MSCs-derived sEVs relies not only on selecting an appropriate cell source, but also on establishing robust, standardized, and reproducible manufacturing conditions. The yield, molecular composition, purity, and biological activity of MSCs-derived sEVs are profoundly influenced by upstream culture parameters, including oxygen tension, passage number, cell density, substrate architecture, nutrient availability, and serum composition (14-16).

Among these factors, serum concentration is one of the most critical variables requiring standardization. Conventional fetal bovine serum (FBS), routinely used for MSC culture, contains high levels of bovine-derived vesicles, soluble proteins, lipoproteins, and growth factors that may co-isolate with cell-derived EVs and interfere with their downstream characterization (17, 18). To address these concerns, exosome-depleted FBS (Exo-free FBS) and/or serum starvation have emerged as preferred strategies in EV-oriented manufacturing workflows. Serum deprivation can activate adaptive stress responses, including autophagy, suppression of mammalian target of rapamycin (mTOR) signaling, metabolic reprogramming, and alterations in endosomal trafficking, potentially affecting multivesicular body formation, vesicle secretion, and cargo loading (19-22). Nevertheless, the effects of serum reduction on EV production and stress signaling remain inconsistent across studies and appear to depend on cell source, the severity and duration of serum restriction, and the EV isolation method (20, 21). This variability underscores the need to systematically investigate the serum-modulation strategies under well-defined, reproducible culture conditions. Additionally, reliable interpretation of serum-induced changes also requires comprehensive characterization of the resulting EV preparations. Current MISEV guidelines emphasize using multiple approaches to characterize EV preparations, including evaluation of particle morphology and size, EV-associated molecular components, and potential non-EV contaminants. Currently, rigorous biological safety evaluation, aligned with ISO 10993 guidelines, is essential for determining the biocompatibility and safety of candidate biologically derived nanoformulations (23, 24).

In recent decades, clinical studies have highlighted the therapeutic potential of MSC-derived EVs for diabetic ulcers, osteoarthritis, neuroinflammation, cardiovascular injury, and immune-mediated disorders. However, their widespread clinical translation requires standardized production strategies, validated isolation methods, consistent batch quality, and robust safety evaluation. Therefore, understanding how manufacturing variables influence both vesicle quality and biological compatibility represents a major translational priority. Despite growing interest in modifying MSC culture conditions to regulate EV production, the effects of progressive serum reduction on AdMSC behavior and the physicochemical and biological characteristics of the resulting EV preparations remain insufficiently defined. Moreover, studies simultaneously examining cellular responses, physicochemical characteristics, and biocompatibility under sequential low-serum conditions remain limited. We therefore hypothesized that controlled stepwise serum reduction would enhance sEV yield, homogeneity, and stability without compromising cell viability or safety (25). Accordingly, this study investigated the effects of progressively reducing exosome-depleted FBS from 10% to 5% and subsequently to 1% over 36 hr, compared with continuous culture in 10% exosome-depleted FBS, on human AdMSCs (total cell density, viability, apoptosis, differentiation potential, and migration capacity) and their secreted sEV-enriched particles. AdMSC-derived sEV-enriched particles were isolated and characterized for morphological characteristics (shape, EV size, topography, distribution), structural properties (hydrodynamic diameter, distribution, surface charge, electrostatic potential, and colloidal behavior), chemical features (functional groups and total protein concentration), and biocompatibility (cytotoxicity, acute systemic toxicity, irritation, and sensitization). To clarify the study design and analytical workflow, Figure 1 presents a schematic overview of the experimental procedure.

Materials and Methods

The Research Ethics Committee of the Islamic Azad University, Science and Research Branch, approved the study under registration ID IR.IAU.SRB.REC.1403.018, in accordance with the Declaration of Helsinki. All chemicals were purchased from Sigma (St. Louis, MO, USA), unless

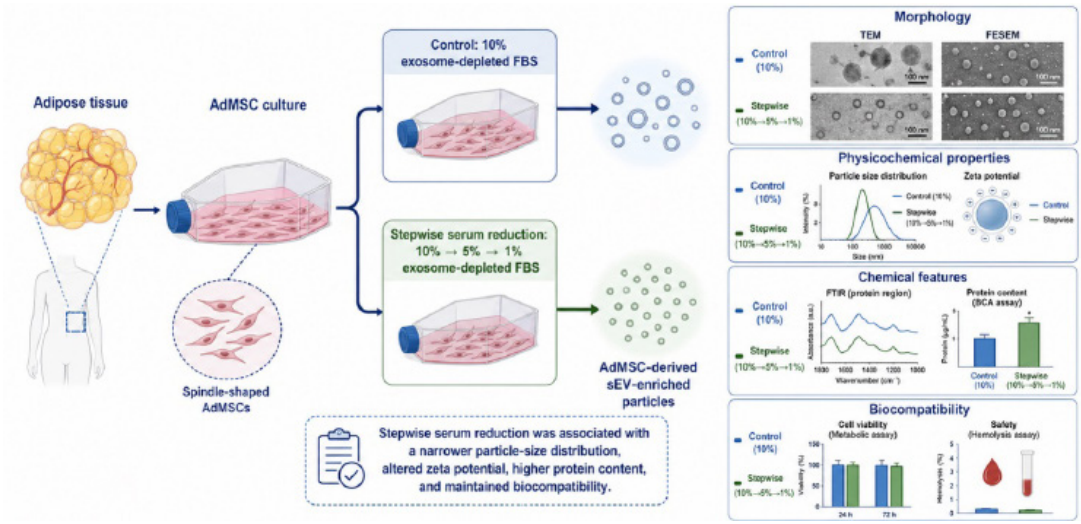


Figure 1. Schematic overview of the study workflow, including adipose-derived mesenchymal stromal cells (AdMSC) isolation and culture, controlled serum reduction, conditioned medium collection, isolation of sEV-enriched particles, physicochemical and morphological characterization, and biocompatibility evaluation

Corrected Proof

otherwise specified.

Human adipose tissues were collected from five healthy donors via selective liposuction at Gandhi Hotel Hospital, Tehran, Iran, according to predefined inclusion and exclusion criteria. Donor inclusion criteria were as follows: age between 23 and 57 years; and the absence of drug addiction, metabolic diseases, liver disorders, bacterial/mycoplasma infections, and viral infections such as HIV, HBV, HCV, and HPLV. All tissue samples were obtained following written informed consent from each participant.

Isolation and proliferation of AdMSCs

Human adipose tissues were collected in sterile containers and transported to the laboratory on ice (4 °C). Tissues were processed using a protocol described by Heidari *et al.* (26) with minor modifications. Briefly, tissues were washed with PBS supplemented with 10% FBS, 100 IU/ml penicillin, and 100 µg/ml streptomycin; minced into small pieces (fibrous tissue removed); and digested with 0.6 mg/ml collagenase type IV at 37 °C for 90–120 min with gentle agitation. The stromal vascular fraction was filtered through a 100-µm nylon mesh, centrifuged at 1,200 × g for 10 min at room temperature, and resuspended in culture medium (DMEM supplemented with 10% FBS, 1% non-essential amino acids (NEAA), 3.7 g/l $NaHCO_3$, 2 mM L-glutamine, 100 U/ml penicillin, and 100 µg/ml streptomycin). Cells were plated at 1×10^6 cells/ml in 75-cm^2 flasks and incubated at 37 °C and 5% CO_2 for 21–28 days (primary culture). Medium was replaced every 3 days until cells reached 80–90% confluence. Confluent cells were trypsinized (0.05% trypsin-EDTA), passaged at the same density, and incubated for 72 hr (passage 1). AdMSCs were subcultured to passage 3, cryopreserved at a cooling rate of −1 °C/min in freezing medium, and stored at −80 °C until use.

Verification of AdMSCs

To confirm AdMSCs at passage 3, we evaluated expression of established MSC-associated surface markers, as previously described by Heidari *et al.* (26). Briefly, 1×10^6 AdMSCs were analyzed using flow cytometry. The expression profiles of three positive MSC markers, CD105, CD29, and CD90, and three negative markers, CD45, CD14, and CD34, were assessed using a flow cytometry.

Study design

Confirmed AdMSCs from the previous section were randomly divided into the control and experimental groups. In the experimental group, AdMSCs were initially cultured in Dulbecco's modified Eagle medium (DMEM) supplemented with 10% exosome-depleted FBS (Exo-free FBS, ThermoFisher, Waltham, MA, USA), 1% NEAA, 3.7 mg/ml $NaHCO_3$, 2 mM L-glutamine, 100 U/ml penicillin, and 100 µg/ml streptomycin for 12 hr. Subsequently, the serum concentration was sequentially reduced from 10% to 5% and then to 1%, with cells maintained at each serum concentration for 12 hr (total culture duration of 36 hr under sequential serum reduction). In the control group, AdMSCs were cultured in DMEM supplemented with 10% exosome-depleted FBS, 1% NEAA, 3.7 mg/ml $NaHCO_3$, 2 mM L-glutamine, 100 U/ml penicillin, and 100 µg/ml streptomycin at 37 °C, 5% CO_2, and 80% humidity for 36 hr. In both groups, the cells were seeded at a density of 1×10^6 cells/ml in 75 cm^2 culture flasks (2×10^6 cells per T75 flask) and incubated at 37 °C, 21% O_2, and 5% CO_2.

Effect of culture conditions on AdMSC characteristics

Concentration and viability of AdMSCs in the control and experimental groups

Confirmed AdMSCs from the previous section were randomly divided into the control and experimental groups. In the experimental group, AdMSCs were suspended in DMEM containing stepwise serum reduction (10%, 5%, and 1% exosome-depleted FBS), 1% NEAA, 3.7 mg/ml $NaHCO_3$, 2 mM L-glutamine, 100 U/ml penicillin, and 100 µg/ml streptomycin. The cells were seeded at 1×10^6 cells/ml in 75 cm^2 culture flasks (2×10^6 cells per T75 flask) and incubated at 37 °C, 21% O_2, and 5% CO_2 for 36 hr.

In the control group, AdMSCs were cultured in DMEM supplemented with 10% exosome-depleted FBS, 1% NEAA, 3.7 mg/ml $NaHCO_3$, 2 mM L-glutamine, 100 U/ml penicillin, and 100 µg/ml streptomycin at 37 °C, 5% CO_2, and 80% humidity for 36 hr.

Stemness potential of AdMSCs in different culture conditions

To evaluate the effect of low-serum conditions on the stemness potential of AdMSCs, their multilineage differentiation into osteocytes, adipocytes, and chondrocytes was assessed, according to the protocol described by Sarvari *et al.* (27). For osteogenic differentiation, AdMSCs were cultured in DMEM supplemented with 50 µg/ml ascorbic acid, 10 nM dexamethasone, and 10 mM β-glycerol phosphate for 28 days. Adipogenic differentiation was induced using DMEM containing 50 µg/ml ascorbic acid, 100 nM dexamethasone, and 50 µg/ml indomethacin. For chondrogenic differentiation, AdMSCs were cultured in DMEM supplemented with 0.1 µM dexamethasone, 50 µg/ml ascorbic acid, and 10 ng/ml TGF-β1 for 21 days. Differentiation into osteocytes, adipocytes, and chondrocytes was confirmed by staining with Alizarin Red, Oil Red O, and Toluidine Blue, respectively. All staining procedures were performed in triplicate to ensure reproducibility.

Migration of AdMSCs under various conditions

Migration of AdMSCs in both control and experimental groups was evaluated using a scratch assay, following a protocol previously established by Karimi *et al.* (28). Briefly, AdMSCs were seeded at a density of 5×10^5 cells per well in 6-well culture plates and incubated for 48 hr in medium supplemented with 1% exosome-depleted FBS for the experimental group and 10% exosome-depleted FBS for the control group. Once the cultures reached 80–90% confluency, a uniform scratch was made across the cell monolayer, and images were captured at 0, 24, and 48 hr after scratching. The scratch area at each time point was quantified using ImageJ software to determine the migration capacity of AdMSCs in both groups. All migration assays were performed in triplicate to ensure consistent, reliable results.

Apoptosis of AdMSCs in different groups

Acridine orange staining was used to semi-quantitatively distinguish apoptosis-associated changes in AdMSCs between the control and experimental groups. To evaluate apoptosis, cultured AdMSCs in both groups were stained with Acridine Orange (5 µg/ml) for 10 min at 37 °C in the dark. Apoptotic cells were semi-quantitatively analyzed using a fluorescence microscope to detect morphological features associated with nuclear integrity and apoptosis in live and apoptotic cells. If AdMSCs exhibit green fluorescence under Acridine Orange staining, the cells are viable, whereas red fluorescence indicates apoptosis. In both groups, all staining was performed in triplicate to ensure reliability.

Corrected Proof

Extraction and characterization of AdMSC-derived sEV-enriched particles under various culture conditions

In the control and experimental groups, AdMSC-derived sEV-enriched particles were isolated from the conditioned media of AdMSCs using a differential ultracentrifugation technique, as previously described by Kholgh *et al.* (29). Briefly, the conditioned media from both groups were collected after 36 hr of culture and centrifuged at 300×g for 10 min at 4 °C to remove residual cells and large debris. After discarding the pellet, the resulting supernatant was centrifuged again at 2,000×g for 30 min to eliminate smaller debris and apoptotic bodies. To ensure complete removal of large vesicles, the supernatant was further centrifuged at 10,000×g for 60 min at 4 °C. Finally, the clarified supernatant was ultracentrifuged at 100,000×g for 70 min at 4 °C, and the resulting pellet containing small extracellular particles was collected. The pellet was gently resuspended in ice-cold PBS, passed through a 0.22 µm sterile membrane filter, and frozen at −80 °C for subsequent analyses. To ensure reproducibility and obtain sufficient AdMSC-derived sEV-enriched particles for subsequent analyses, the ultracentrifugation-based extraction was repeated at least 7 times for each group (7 preparations for the control group and 7 for the experimental group). The same standard operating procedure (SOP) was used for each preparation. The seven preparations from each group were pooled separately to obtain the control and experimental particle preparations, which were subsequently used for subsequent analyses.

Morphological characteristics of AdMSC-derived sEV-enriched particles

The morphological characteristics, including dry size, internal structure, and topography of AdMSC-derived sEV-enriched particles, were detected in the control and experimental groups using Field Emission Scanning Electron Microscopy (FESEM) and Transmission Electron Microscopy (TEM), as described previously by Kholgh *et al.* (29).

For FESEM analysis, 500 µl of the suspension containing sEV-enriched particles was fixed in 2% paraformaldehyde and diluted in distilled water. Then, 5 µl of the suspension was placed on a silicon chip and immersed in acetone for dehydration. After rinsing and drying, FESEM was performed at 30 kV using a MIRA3 microscope (TESCAN, Czech Republic). For image acquisition and analysis, ten randomly selected fields were evaluated at magnifications of 20 µm, 5 µm, and 500 nm.

For TEM analysis, 500 µl of the AdMSC-derived sEV-enriched suspension was fixed with 1% glutaraldehyde and deposited as droplets onto carbon-coated grids, then allowed to adsorb. After drying for 2 min, the grids were rinsed twice with sterile PBS for 1 min and negatively stained with 1% uranyl acetate for 16 min before imaging using a Philips CM-120 transmission electron microscope (Netherlands) at an accelerating voltage of 100 kV. Multiple fields were examined at magnifications of 50 nm and 100 nm. TEM and FESEM were repeated in triplicate for each group, and at least ten randomly selected fields were assessed.

Chemical features of AdMSC-derived sEV-enriched particles

Fourier Transform Infrared Spectroscopy (FTIR) provided detailed information on the molecular composition and functional groups of AdMSC-derived sEV-enriched particles under different culture conditions through their infrared absorption profiles. For FTIR analysis, 500 µl of particle suspensions from each group (control and experimental) were analyzed in triplicate using an AVATAR spectrometer (Thermo, USA), and the spectral data were analyzed in the range of 400–4000 cm^{-1}. This analysis determined the biochemical composition of AdMSC-derived sEV-enriched particles and highlighted similarities and differences in molecular structure between sEV-enriched particles from control and experimental groups.

To evaluate the biochemical characteristics of AdMSC-derived sEV-enriched particles, the Bradford protein assay was used to quantify the total protein concentrations in both control and experimental groups. For each group, 500 µl of particle suspension was analyzed in triplicate using a commercial Bradford assay kit (Bio-Rad). The assay is based on Coomassie Brilliant Blue dye binding to proteins, and the resulting colorimetric response was used to determine total protein concentration.

Structural properties of AdMSC-derived sEV-enriched particles

The hydrodynamic diameter, distribution, surface charge, and electrostatic potential of AdMSC-derived sEV-enriched particles in both the control and experimental groups were measured using Dynamic Light Scattering (DLS) and zeta potential measurements with the HORIBA SZ-100 system (Horiba Jobin Yvon, Japan), following the method previously described by Karimi *et al.* (30). For this purpose, 1000 µl of the extracted sEV-enriched particle suspension was diluted fivefold with PBS and sonicated on ice for 20 min to ensure adequate homogenization. Zeta potential measurements were conducted at pH 7.4, 25 °C, and 2.7 V. All measurements were performed in triplicate to ensure data reproducibility and reliability.

Biocompatibility of AdMSC-derived sEV-enriched particles

The biocompatibility of AdMSC-derived sEV-enriched particles was investigated through a series of comprehensive assessments, including microbial contamination, cytotoxicity, acute systemic toxicity, irritation, and sensitization assays. To ensure reproducibility and reliability, microbial contamination, cytotoxicity, and *in vivo* biocompatibility tests (irritation, sensitization, and acute systemic toxicity assessments) were independently performed by Nikopharmed's laboratories, a reputable partner of the Food and Drug Administration (FDA), with official accreditation from the National Accreditation Center of Iran (NACI). In vivo irritation, sensitization, and acute systemic toxicity assays were conducted using three male New Zealand rabbits, six male albino guinea pigs, and twelve NMRI mice. For each analysis, 10 ml of the AdMSC-derived sEV-enriched particle suspension in each group was transported to the laboratory under cold conditions (on ice). Each biocompatibility analysis was independently performed in triplicate.

In vivo irritation assay of AdMSC-derived sEV-enriched particles in male new Zealand rabbits

The *in vivo* irritation test of AdMSC-derived sEV-enriched particles was conducted at Nikopharmed's laboratories, a reputable partner of the Food and Drug Administration (FDA), with official accreditation from the National Accreditation Center of Iran (NACI), in accordance with ISO 10993-23 and ISO 10993-12 guidelines. For this purpose, three male New Zealand rabbits (aged 2–3 months;

Corrected Proof

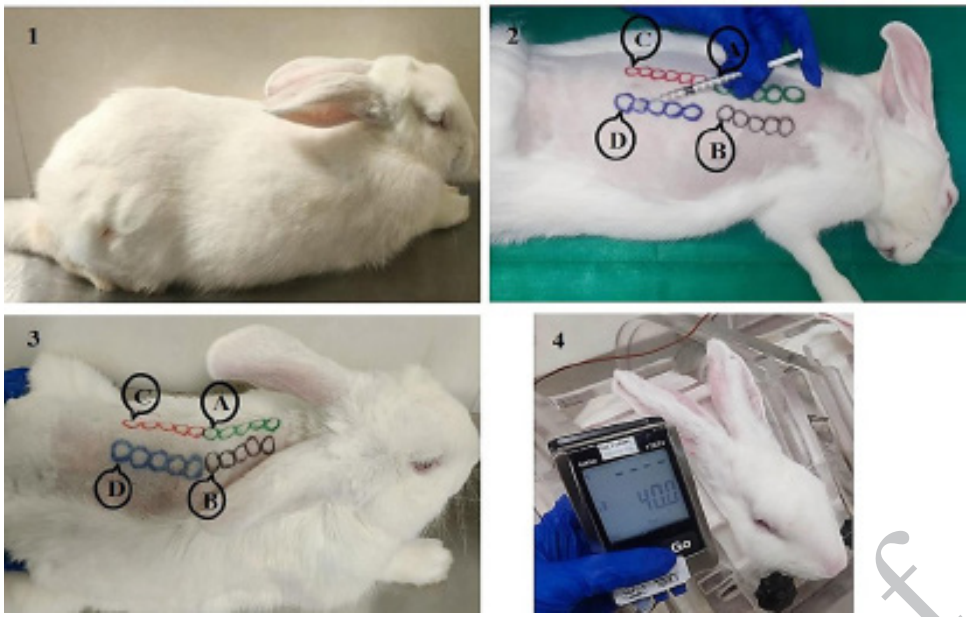


Figure 2. Preparation of male New Zealand rabbits for the test (1), with shaving of the animals' backs and highlighting 20 injection sites (10 on each side) as colored circles (2). Intradermal injection of AdMSC-derived sEV-enriched particles from the control group at a concentration of 0.2 ml, dissolved in a nonpolar solvent (green circles); AdMSC-derived sEV-enriched particles from the control group dissolved in a 0.9% polar sodium chloride solution (red circles); AdMSC-derived sEV-enriched particles from the experimental group dissolved in a nonpolar corn oil solvent (black circles); AdMSC-derived sEV-enriched particles from the experimental group dissolved in a polar sodium chloride solution (blue circles); polar sodium chloride solution (sites A and B); and nonpolar corn oil solution (sites C and D) in the New Zealand rabbits (2, 3). Evaluation of rabbits' body temperature before and after AdMSC-derived sEV-enriched particle injections (4).

weight>2 kg) were housed under controlled conditions of 22±3 °C, 55±10% humidity, and a 12-hr light/12-hr dark cycle. The dorsal hair of the rabbits was carefully shaved, and 20 injection sites (10 on each side) were marked as colored circles (Figure 2). AdMSC-derived sEV-enriched particles from the control group (0.2 ml) were dissolved in a nonpolar solvent (corn oil) and subcutaneously injected into the upper left flank (green circles). In the lower left flank (red circles), animals received a subcutaneous injection of 0.2 ml of AdMSC-derived sEV-enriched particles from the control group dissolved in a polar solution (0.9% sodium chloride). Injections of AdMSC-derived sEV-enriched particles from the experimental group, dissolved in a nonpolar solvent (corn oil), were performed on the upper right side of the animals (black circles). Additionally, blue circles in the lower right flanks received 0.2 ml of AdMSC-derived sEV-enriched particles from the experimental group dissolved in 0.9% polar sodium chloride solution. Sites A and B received 0.2 ml of polar sodium chloride solution, while sites C and D received the same volume (0.2 ml) of nonpolar corn oil solvent (Figure 2). *In vivo* irritation responses, including edema, erythema, and eschar formation, were evaluated at 24±2, 48±2, and 72±2 hr post-injection. The scoring criteria for local tissue reactions are presented in Table 1. Based on the primary irritation index (PII), irritation responses were classified into four categories: negligible (0–0.4), representing the acceptable range; slight irritation (0.5–1.9); moderate irritation (2.0–4.9); and severe irritation (5.0–8.0). Furthermore, the animals' body temperatures were measured before and after injections using a calibrated measurement device with an accuracy of ±0.1 °C. Body temperatures were recorded every 30 min for up to 180 min post-injection. A temperature difference not exceeding 0.6 °C between pre- and post-injection measurements was considered acceptable according to the predefined temperature assessment criterion.

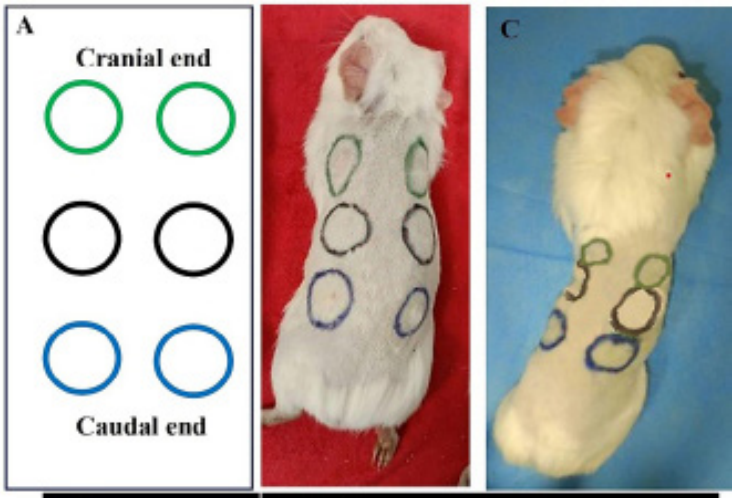
In vivo sensitization assay of AdMSC-derived sEV-enriched particles in male albino guinea pigs

Nikopharmed's laboratories, a reputable FDA partner with official NACI accreditation, performed an *in vivo* irritation

Table 1. Scoring system in the *in vivo* irritation test of New Zealand rabbits

Reactions		
Edema	Erythema	Eschar formation
0 (No edema)	0 (No erythema)	0 (No eschar)
1 (Very slight edema; barely perceptible)	1 (Very slight erythema; barely perceptible)	1 (Very slight eschar)
2 (Well-defined edema by definite raising)	2 (Well-defined erythema)	2 (Well-defined eschar)
3 (Moderate edema; raised approximately 1 mm)	3 (Moderate erythema)	3 (Moderate eschar)
4 (Severe edema; raised more than 1 mm and extending beyond the exposure area)	4 (Severe erythema; beet-redness)	4 (Severe eschar formation)
8 (Maximal edema for Irritation)		

Corrected Proof



Sites	Solution
Green circles	0.1 ml of sEVs in the control group
Black circles	0.1 ml of 0.9% sodium chloride
Blue circles	0.1 ml of sEVs in the experimental group

Figure 3. Schematic diagram (A) of the intradermal injection sites for adipose-derived mesenchymal stromal cells (AdMSC)-derived sEV-enriched particles in Albino guinea pigs, and representative images of the control group (B) and experimental group (C). In both groups, the green circles received 0.1 ml of AdMSC-derived sEV-enriched particles from the control group, the black circles received 0.1 ml of 0.9% sodium chloride, and the blue circles received 0.1 ml of AdMSC-derived sEV-enriched particles from the experimental group

test for AdMSC-derived sEV-enriched particles in both the control and experimental groups in accordance with ISO 10993-10, ISO 10993-12, and ISO 10993-2 guidelines. A total of six male Albino guinea pigs (4–5 months old; 300–500 g body weight) were used for the *in vivo* sensitization test and maintained under controlled environmental conditions at 21±3 °C, 50±10% humidity, and a 12-hr light/dark cycle. The animals received standard chow and water *ad libitum*, and their cages were cleaned daily. For the sensitization assay, the dorsal hair of the animals was completely shaved, and six injection sites were marked with colored circles, as illustrated in Figure 3. The sites marked with black circles received intradermal injections of 0.1 ml (100 µl) of 0.9% sodium chloride solution. The sites marked with green circles received the same volume of AdMSC-derived sEV-enriched particles from the control group, whereas those marked with blue circles received AdMSC-derived sEV-enriched particles from the experimental group. Local skin reactions, including edema, erythema, and eschar formation, were evaluated at 24±2, 48±2, and 72±2 hr post-injection. Skin responses were graded according to the Magnusson and Kligman scoring system, using a four-point scale: 0, no visible change; 1, discrete or patchy erythema; 2, moderate and confluent erythema; and 3, intense erythema and/or swelling.

Cytotoxicity assessment of AdMSC-derived sEV-enriched particles on L929 mouse fibroblasts

Following ISO 10993-5 guidelines, we assessed the viability and morphological characteristics of L929 mouse fibroblasts (NCTC clone 929) treated with AdMSC-derived sEV-enriched particles from both the control and experimental groups using the MTT assay. Analyses were performed at Nikopharmed's laboratories, a reputable FDA partner with official NACI accreditation. For the cytotoxicity assay, L929 mouse fibroblasts were seeded in a 96-well culture plate at a density of 1×10^4 cells per well and cultured in 100 µl of DMEM containing 1% exosome-depleted FBS for the experimental group and 10% exosome-depleted FBS for the control group. The culture plates were incubated at 37 °C in 5% CO_2 for 24 hr. Then, 50 µl of culture medium in each group was replaced with 50 µl of MTT solution. The plates were then returned to incubation at 37 °C in 5% CO_2 for 2 hr. The viable and proliferating cells were quantified by measuring absorbance at 570 nm using a multi-mode microplate reader spectrophotometer (FLUOstar Omega, BMG LABTECH, Ortenberg, Germany). Cell toxicity and viability were determined and calculated using the following formula:

$$\text{Toxicity (\%)} = \left(1 - \frac{\text{mean OD of sample}}{\text{mean OD of control}}\right) \times 100$$

$$\textit{Viability (\%)} = 100 - \%\,\textit{Toxicity}$$

For morphological analysis, L929 mouse fibroblasts were fixed with 2% paraformaldehyde, stained with Giemsa stain (Merck, Darmstadt, Germany), and evaluated using a Nikon Eclipse 50i light microscope. The morphological characteristics of the cells were quantitatively graded on a scale of 0 (intact cells with no signs of intracellular granules, disintegration, or growth retardation) to 4 (severely damaged and destroyed cell layers), with intermediate scores defined as follows:

Score 1 (Mild): Less than 20% of cells are rounded with poor surface adhesion, and there are no significant intracellular granules, cytoplasmic vacuolation, or nuclear changes.

Score 2 (Moderate): 20–50% of cells exhibit rounding without observable intracellular granules, and growth inhibition is moderate, not exceeding 50% of control growth.

Score 3 (Significant): More than 70% of cells are rounded and destroyed, and growth inhibition exceeds 50% of

Corrected Proof

control growth.
Score 4 (Severe): Cell layers are extensively damaged or destroyed, with minimal intact cells remaining. Signs of cell lysis, fragmentation, or complete loss of cellular architecture are observed.

Acute systemic toxicity assessment of AdMSC-derived sEV-enriched particles in NMRI mice

Acute systemic toxicity of AdMSC-derived sEV-enriched particles between different groups was conducted at Nikopharmed's laboratories, a reputable partner of the FDA with official accreditation from the NACI, in accordance with ISO 10993-11, ISO 10993-12, and ISO 10993-2 guidelines. Twelve female and male NMRI mice, each 6–8 weeks old and weighing 25–30 gr, were individually housed in cages under controlled conditions of 22±3 °C, 55±10% humidity, and a 12-hr light/12-hr dark cycle. AdMSC-derived sEV-enriched Particles from both the control and experimental groups were injected subcutaneously at a single dose of 50 ml/kg. Following administration, body weights and clinical signs were monitored at least twice daily before and 72 hr after injection. Mortality, significant clinical abnormalities, or treatment-related adverse effects were considered indicators of systemic toxicity.

Microbial contamination and quality control of AdMSC-derived sEV-enriched particles

In accordance with the United States Pharmacopeia 2024 guidelines, Nikopharmed's laboratories, a reputable FDA partner with official NACI accreditation, performed the bioburden assessment of AdMSC-derived sEV-enriched particles from both the control and experimental groups. Samples from each group were inoculated into nutrient broth carrier solutions using sterile swabs and subsequently cultured on Blood Agar (BA), Eosin Methylene Blue (EMB) Agar, and Chocolate Agar to evaluate the presence of Gram-positive or Gram-negative bacteria. The Total Aerobic Microbial Count (TAMC) was determined using Soybean-Casein Digest Agar incubated at 30–35 °C for 3 days. The Total Combined Yeasts and Molds Count (TYMC) was assessed using Sabouraud Dextrose Agar incubated at 20–25 °C for 5 days. AdMSC-derived sEV-enriched particles passed the microbiological tests if no colonies of specified microbial types were detected or if confirmatory identification tests were negative. To ensure accuracy and reliability, acceptance criteria for microbiological quality were defined based on the mean values of triplicate measurements.

Statistical analysis

Statistical analyses were performed using IBM SPSS Statistics version 22.0 (IBM Corp., Armonk, NY, USA) and GraphPad Prism version 9.0 (GraphPad Software, San Diego, CA, USA). Quantitative data are presented as mean ± standard deviation (SD), whereas qualitative data are expressed as frequency and percentage. Normality of data distribution was assessed using the Shapiro–Wilk test. Comparisons between the control and experimental groups were performed using the independent-samples t-test for normally distributed data and the Wilcoxon test for non-normally distributed data. For quantitative morphological parameters obtained from FESEM analysis, the independent-samples t-test was used for normally distributed data and the Wilcoxon test when the normality assumption was not met. A P-value≤0.05 was considered statistically significant.

Results

Preparation and validation of AdMSCs in both the control and experimental groups

Approximately 1.8–1.9×10^5 MSCs were isolated from each gram of human adipose tissue. Figure 3 illustrates the morphological characteristics of AdMSCs at passage 3 over a 72-hr culture period. The cells appeared spindle- or triangular-shaped, with prominent elliptical nuclei, firmly attached to the bottom of the culture plate. Throughout the culture period, AdMSCs maintained their characteristic fibroblast-like morphology, confirming the preservation of the MSC phenotype during expansion. Cell density gradually increased and reached approximately 40–45%, 70–75%, and 100% after 24, 48, and 72 hr, respectively (Figure 4). At 72 hr post-cultivation, the total number of AdMSCs was 47.45×10^6 and 47.75×10^6 cells in the control and experimental groups, respectively.

Total concentration and viability rates of AdMSCs did not differ significantly between the control and serum starvation groups (P>0.05). Viability was also 99% across groups (P>0.05). Serum starvation did not adversely affect AdMSC quantity or viability. Figure 5 shows AdMSC expression of positive (CD105, CD90, and CD29) and negative (CD45, CD14, and CD34) molecular markers. Positive biomarkers CD105, CD90, and CD29 were highly expressed (100%, 98.2%, and 98.8%, respectively), while negative biomarkers CD45, CD34, and CD14 showed negligible expression (0.1%, 0.022%, and 0.012%, respectively), indicating the purity of the AdMSC population (Figure 5).

Stemness potential of AdMSCs under various culture conditions

AdMSCs in both the control and experimental groups can differentiate into osteocytes, adipocytes, and chondrocytes (Figure 5). AdMSC differentiation potential did not differ significantly between groups (P>0.05). Calcium deposition in osteocytes, accumulation of purple-stained glycosaminoglycans in chondrocytes, and red-colored intracellular lipid vesicles in adipocytes confirmed the stemness potential of propagated AdMSCs in the control and serum-starved groups (Figure 6).

Migration of AdMSCs in the control and experimental groups

Figure 6 illustrates the migratory potential of AdMSCs under different culture conditions at 0, 24, and 48 hr post-scratching. At 0 hr, the mean scratch areas for the control and experimental groups were 246.320±66.92 and 249.256±33.61, respectively. After 24 and 48 hr, the scratch area in the control group decreased to 161.925±21.27 and 34.325±13.93 (reductions of 34.26% and 86.06%), respectively. In contrast, the experimental group exhibited a more pronounced decrease in scratch area (P<0.01, Figure 7). The mean scratch areas in the experimental group reduced to 124.933±43.04 and 13.584±5.15 (reductions of 49.88% and 94.55%), respectively. Statistical analysis revealed a significant difference in migration rates between the groups at 24 and 48 hr, with the experimental group showing significantly higher scratch closure than the control group (P<0.01, Figure 7).

Corrected Proof

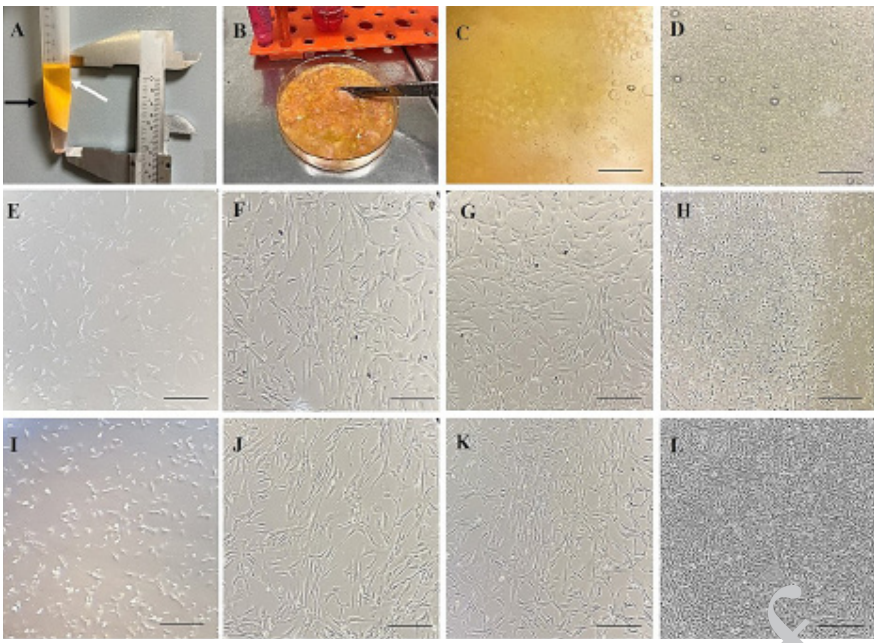


Figure 4. Preparation and culture of human adipose-derived mesenchymal stem cells (AdMSCs)
Initial preparation of adipose tissue; the white arrow indicates the oil layer, and the black arrow denotes the tissue after washing to remove connective tissue, debris, and blood (A). Dissection of adipose tissue and mincing into small pieces (B); adipose tissue after enzymatic digestion (C); suspension of the stromal vascular fraction in culture media (D); proliferation and morphological characteristics of AdMSCs after 12 (E, I), 24 (F, J), 48 (G, K), and 72 (H, L) hr in both the control (E–H) and experimental (I–L) groups at 200× magnification.

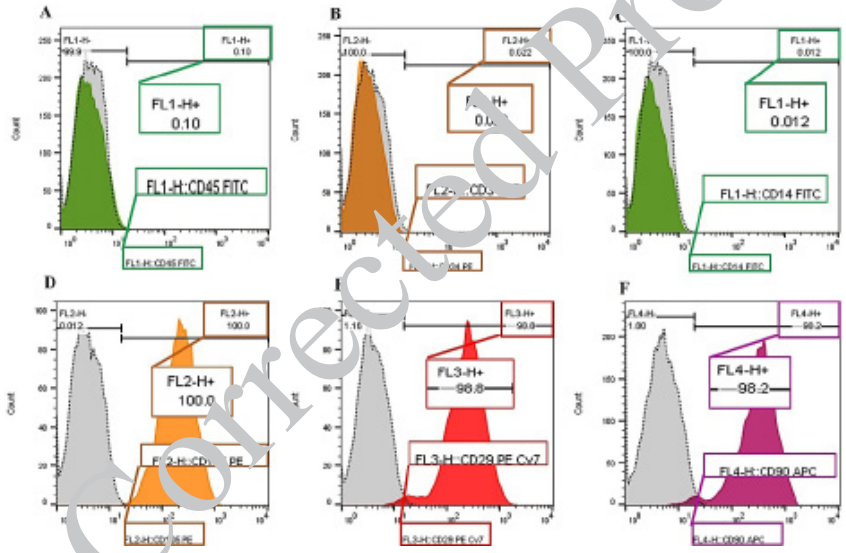


Figure 5. Flow cytometric characterization of adipose-derived mesenchymal stem cells (AdMSCs)
Expression of the negative markers CD45 (A), CD34 (B), and CD14 (C), and the positive MSC-associated markers CD105 (D), CD29 (E), and CD90 (F). The expression of MSC markers were 0.10% for CD45, 0.022% for CD34, 0.012% for CD14, 100% for CD105, 98.8% for CD29, and 98.2% for CD90

Corrected Proof

Apoptosis of AdMSCs under different culture conditions

Figure 8 presents the subjective and semi-quantitative assessment of the apoptotic effect of different culture conditions on AdMSCs under both control and experimental conditions. No statistically significant difference in apoptotic AdMSCs was observed between the control and experimental groups (P>0.05). Cells in both groups predominantly showed green fluorescence with preserved nuclear morphology, with no obvious increase in apoptosis-associated morphological alterations. Furthermore, sequential serum starvation in the experimental group did not induce toxicity in the cultured AdMSCs, nor did it significantly increase the percentage of cells exhibiting apoptosis-associated morphological changes compared to the control group (P>0.05, Figure 8).

Morphological characteristics of AdMSC-derived sEV-enriched particles: Dry size, internal structure, and topography

FESEM analysis characterized the dry size, shape, and surface topography of sEVs from AdMSCs under both control and experimental conditions, as demonstrated in Figure 8. The groups differed significantly in average dry size, structure, and dispersion pattern of AdMSC-derived sEV-enriched particles (P≤0.05). Specifically, the dispersion of extracted AdMSC-derived sEV-enriched particles in the experimental group was significantly lower than in the control group, indicating greater homogeneity and uniformity of nanoparticles in the experimental group compared to the control group (Figures 9D and 9d, P≤0.05). Extracellular vesicles in the control

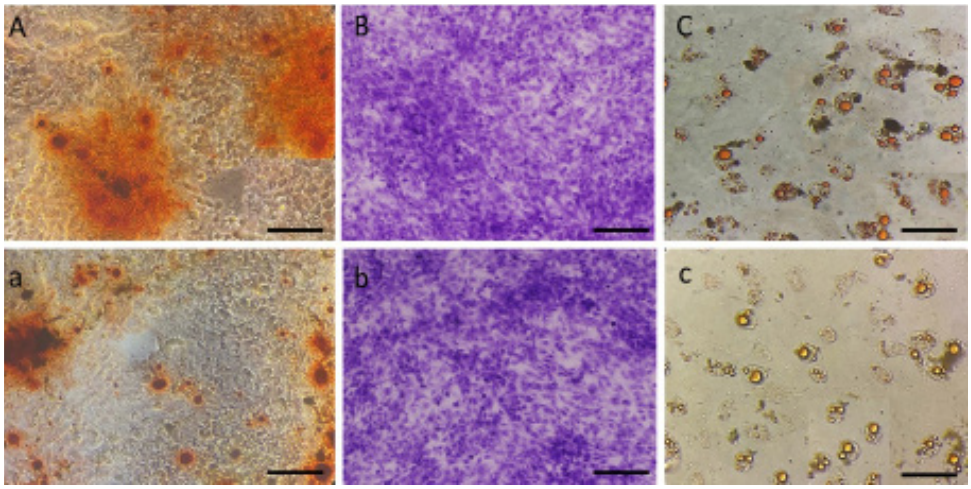


Figure 6. Differentiation of adipose-derived mesenchymal stem cells (AdMSCs) into osteocytes (A, a), chondrocytes (B, b), and adipocytes (C, c) in the experimental (A–C) and control (a–c) groups at 200× magnification

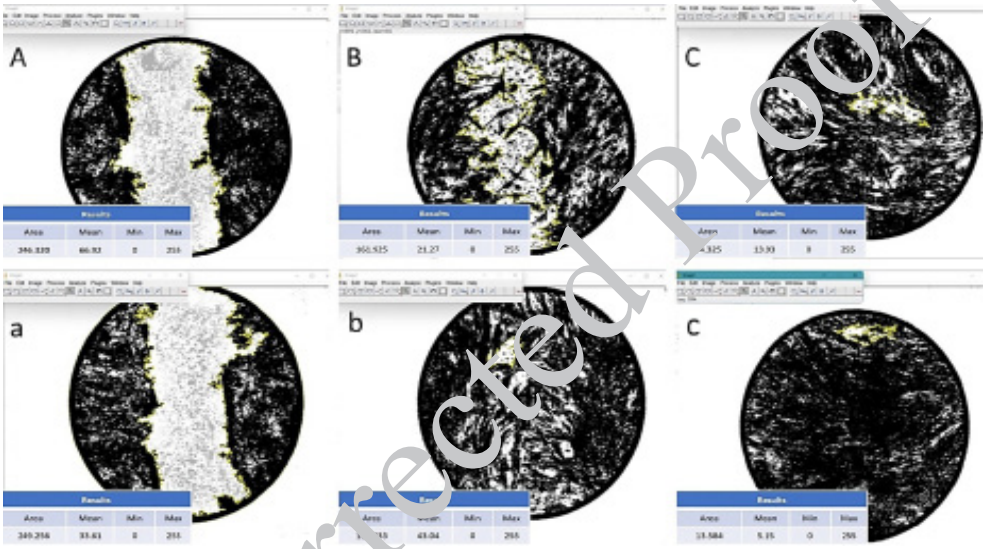


Figure 7. Representative light microscopy images of the scratch wound healing assay showing the migration of adipose-derived mesenchymal stem cells (AdMSCs) in the control (A–C) and experimental (a–c) groups at 0 (A, a), 24 (B, b), and 48 (C, c) hr after scratching. Images were captured using an inverted light microscope at 40× magnification, and the scratch areas were quantified using ImageJ software

Corrected Proof

group displayed two dispersion size distributions of 200±35 to 300±43 nm and 400±17 to 500±23 nm, with the histogram indicating a mean dry size range of 340±14 to 350±12 nm (Figure 9d). However, the nanoparticles in the experimental group showed more coherent, uniform dispersion, with a histogram peak at 47±15 to 49±13 nm (Figure 9D). These findings strongly corroborate the dynamic light scattering (DLS) results for both the control and experimental groups

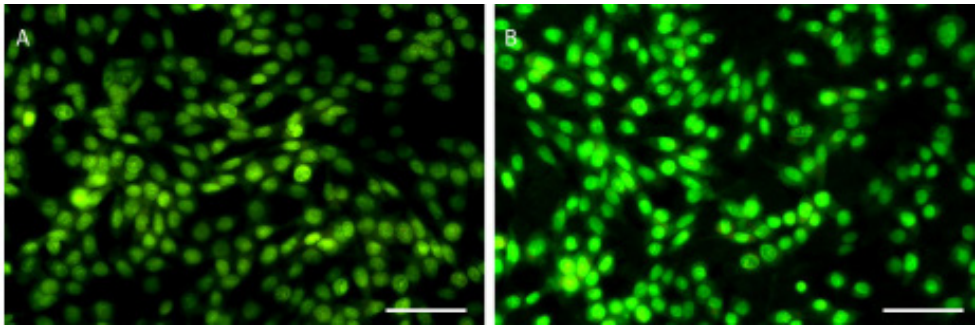


Figure 8. Representative fluorescence microscopy images of acridine orange (AO)-stained adipose-derived mesenchymal stem cells (AdMSCs) in the control (A) and experimental (B) groups for the assessment of apoptosis-associated morphological changes. Images were acquired using a fluorescence microscope at 400× magnification

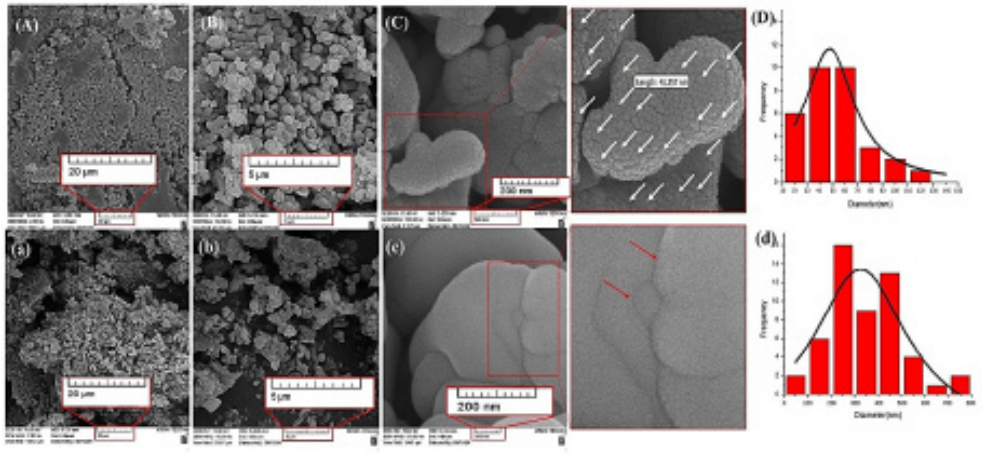


Figure 9. Field emission scanning electron microscopy (FESEM) analysis of the dry size, morphology, and dispersion of adipose-derived mesenchymal stem cells (AdMSCs)-derived sEV-enriched particles in the experimental (A–D) and control (a–d) groups

The experimental group (A–D) showed relatively homogeneous, uniformly dispersed particles (white arrows), predominantly small vesicles with a narrower size distribution (D). In contrast, the control group (a–d) exhibited a broader particle distribution, including larger extracellular vesicle-like structures and aggregates (red arrows) (d). Representative FESEM images are shown at scale bars of 20 µm (A, a), 5 µm (B, b), and 200 nm (C, c).

($P \leq 0.05$, Figure 9).

Structural characteristics of AdMSC-derived sEV-enriched particles; surface topography and aggregation

Figure 10 shows the surface topography, dispersion, and aggregation of extracellular vesicles in both the control and experimental groups. In TEM analysis, AdMSC-derived sEV-enriched particles appear as hollow spherical particles with a distinct lipid bilayer (white arrows, Figure 10). Extracellular vesicles differed significantly in size, dispersion, and aggregation between the control and experimental groups ($P \leq 0.05$). In the control group, extracellular vesicles were significantly larger, more dispersed, and more susceptible to aggregation and agglomeration (red arrows and arrowheads, Figures 10a and 10b). In contrast, AdMSC-derived sEV-enriched particles in the experimental group showed uniform dimensions and a more homogeneous distribution, indicating reduced aggregation compared with the control group (white arrows, Figures 10A and 10 B) ($P \leq 0.05$).

Chemical characteristics of AdMSC-derived sEV-enriched particles; functional groups and ionic interactions

Figure 11 shows the chemical composition and functional groups of AdMSC-derived sEV-enriched particles from both the experimental and control groups. FTIR analysis confirmed that AdMSC-derived sEV-enriched particles in both groups consisted of various biomolecules, including proteins, lipids, and glycoproteins. The most important absorption peaks were observed at 3419.95 cm^{-1} and 2920.15 cm^{-1}, corresponding to amine (N–H) and hydroxyl (O–H) groups, respectively. Peaks at 2854.50 cm^{-1} (C–H bonds) and 1654.47 cm^{-1} (C=O bonds) confirmed the presence of lipids and proteins. Additional peaks at 1541.15 cm^{-1} and 1122.61 cm^{-1} indicated the presence of amide and phosphate groups, respectively. The 629.47 cm^{-1} band, related to C–H bonds in aromatic rings, emphasizes the

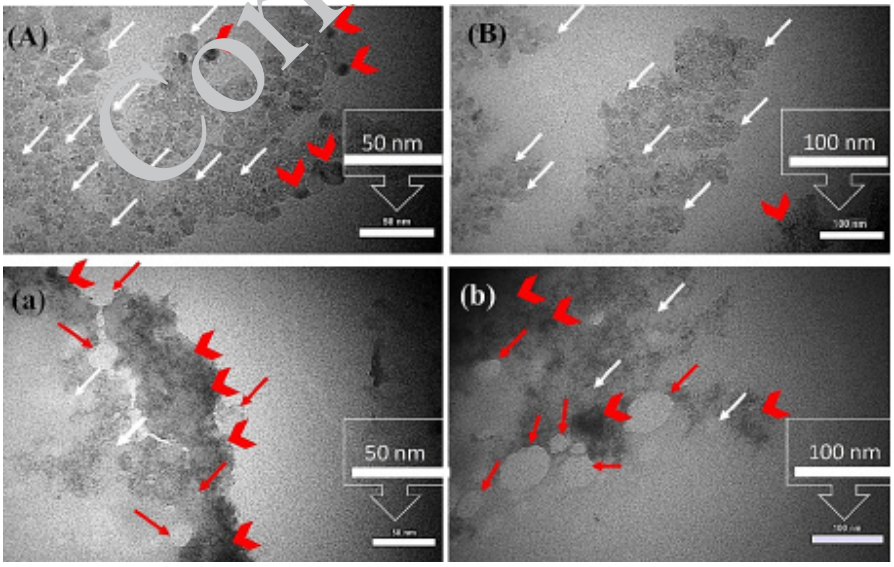
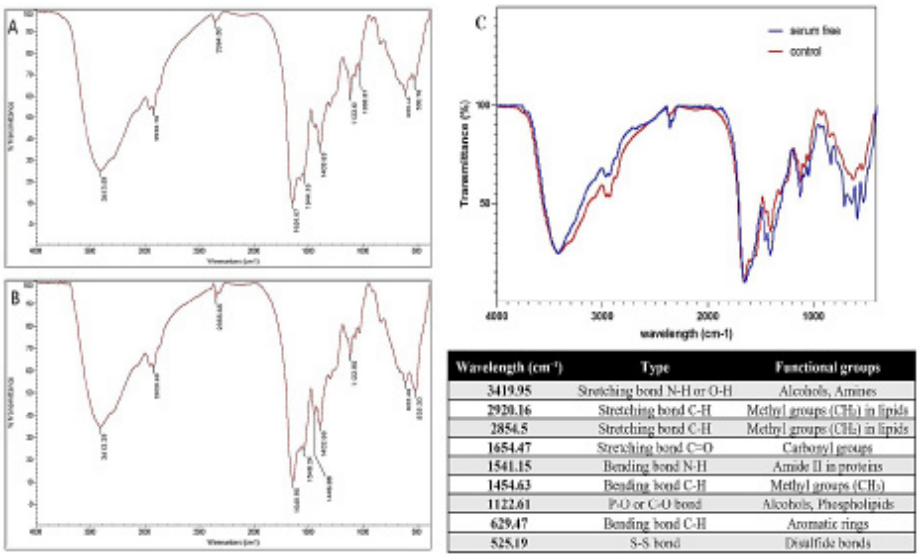


Figure 10. Transmission electron microscopy (TEM) analysis of the aggregation, surface morphology, and dispersion of extracellular particles in the experimental (A, B) and control (a, b) groups

White arrows indicate AdMSC-derived sEV-enriched particles, red arrows indicate larger-sized extracellular vesicles, and red arrowheads highlight prominent vesicle agglomeration. The experimental group showed predominantly smaller, more uniformly dispersed particles, whereas the control group showed larger vesicular structures with greater aggregation. Scale bars represent 50 nm in panels A and a and 100 nm in panels B and b.

Corrected Proof



Wavelength (cm^{-1})	Type	Functional groups
3419.95	Stretching bond N-H or O-H	Alcohols, Amines
2920.16	Stretching bond C-H	Methyl groups (CH_3) in lipids
2854.5	Stretching bond C-H	Methyl groups (CH_2) in lipids
1654.47	Stretching bond C=O	Carbonyl groups
1541.15	Bending bond N-H	Amide II in proteins
1454.63	Bending bond C-H	Methyl groups (CH_3)
1122.61	P-O or C-O bond	Alcohols, Phospholipids
629.47	Bending bond C-H	Aromatic rings
525.19	S-S bond	Disulfide bonds

Figure 11. Comparison of FTIR spectral profiles of AdMSC-derived sEV-enriched particles in the control group (A), experimental group (B), and overlaid comparison of both groups (C), showing similarities and differences in their characteristic absorption bands

complexity of the sEV structure.

Although some peaks differed between the control and experimental groups, these variations were not statistically significant (Figure 11c, $P>0.05$).

Biochemical properties of AdMSC-derived sEV-enriched particles; total protein concentration

Total protein concentration of extracted AdMSC-derived sEV-enriched particles was determined using the Bradford method (Figure 12). Total protein concentration differed significantly between the control and experimental groups ($P\leq0.05$). Specifically, the control group showed a protein concentration of 2.1754 mg/ml. In comparison, the experimental group had a substantially higher concentration of 4.34699 mg/ml, nearly doubling that of the control ($P\leq0.05$, Figure 12).

Physical properties of AdMSC-derived sEV-enriched particles; hydrodynamic diameter, distribution, and behavior of colloidal particles

Figure 12 shows the hydrodynamic diameter, behavior, and distribution of colloidal sEV-enriched particles in the control and experimental groups. The two groups differed significantly in particle size, Z-average, and behavior ($P<0.01$). AdMSC-derived sEV-enriched particles in the control group showed a polydisperse distribution, whereas those in the experimental group showed a monodisperse pattern.

In the control group, we demonstrated two distinct particle-size populations. In this group, the predominant population (approximately 80%) had a mean hydrodynamic diameter of 223.7±45.7 nm. In contrast, the mode (the most frequently observed particle diameter) was 229.8 nm, indicating that this diameter represented the predominant particle population. The remaining 20% of the control group population had a substantially smaller hydrodynamic diameter, with a mean of 50.8±5.7 nm and a mode of 49.1 nm. In contrast, the most AdMSC-derived sEV-enriched particles in the experimental group averaged 34.1±3.1 nm, with a mode of 34.1 nm (Figure 13).

Furthermore, analysis of scattered-light fluctuations, as shown in the correlation diagram, showed significantly greater fluctuations in the control group than in the experimental group ($P\leq0.05$). Generally, when the particles in solution are small, uniformly dispersed, and colloidally stable, with a low tendency to aggregate, their light-scattering behavior is more consistent, resulting in lower and more stable fluctuations in scattered-light intensity. Conversely, when particles are heterogeneous and more prone to aggregation or agglomeration, larger and more irregular fluctuations in scattered-light intensity are detected. Thus, the magnitude and pattern of scattered-light fluctuations can provide indirect information about particle dispersion, heterogeneity, and colloidal stability within the suspension. In the present study, the lower scattered-light fluctuations of nanoparticles in the experimental group were consistent with greater colloidal stability, more uniform particle dispersion, and a reduced tendency for particles to aggregate. In contrast, the higher fluctuations observed in the control group may indicate greater particle heterogeneity, reduced colloidal stability, and a greater tendency toward aggregation and agglomeration ($P\leq0.05$).

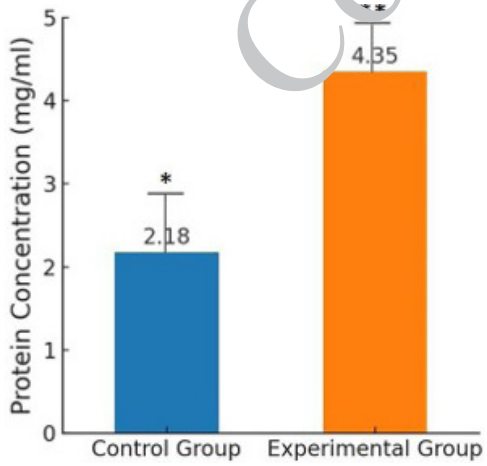


Figure 12. Total protein concentration of adipose-derived mesenchymal stem cell (AdMSC)-derived sEV-enriched particles in the control and experimental groups

Corrected Proof

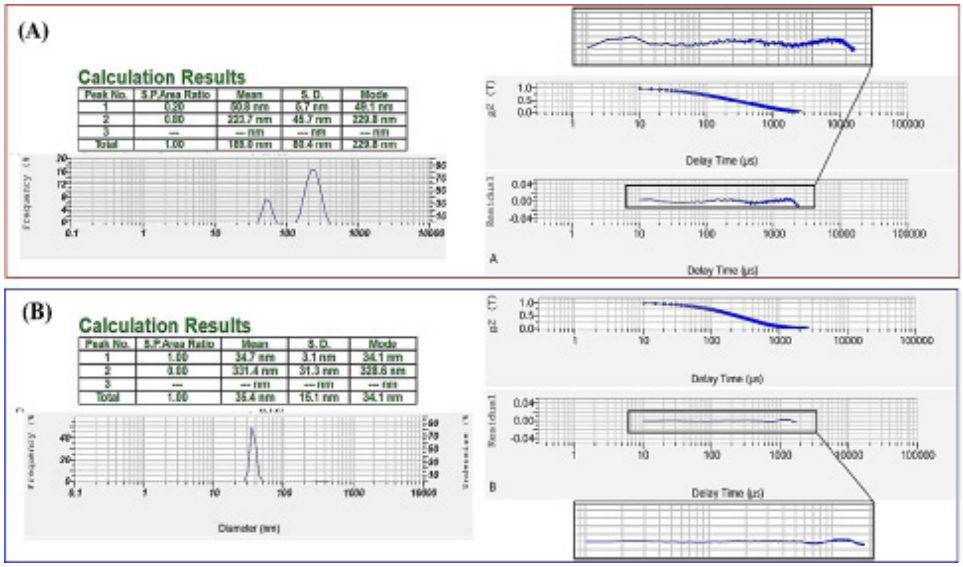


Figure 13. Hydrodynamic diameter, colloidal behavior, and dispersion characteristics of sEV-enriched particles in the control (A) and experimental (B) groups, as determined by dynamic light scattering (DLS)
The left panels show the particle-size distribution, indicating a polydisperse population in the control group and a more homogeneous, monodisperse population in the experimental group, along with the mean particle diameter (Mean±SD) and the most frequently observed particle size (mode) for each group. The right panels show the scattered-light fluctuation analysis, revealing greater fluctuations and a higher tendency toward nanoparticle aggregation and agglomeration in the control group (A) than in the experimental (B) group.

Structural properties of AdMSC-derived sEV-enriched particles; surface charge, electrophoretic mobility, and stability

Figure 14 shows the zeta potentials of AdMSC-derived sEV-enriched particles in the control and experimental groups. AdMSC-derived sEV-enriched particles in the control group had an average zeta potential of −4.9 mV and a mean electrophoretic mobility of −0.000038 cm^2/Vs In contrast, the experimental group exhibited a more negative zeta potential of −9.0 mV with an electrophoretic mobility of −0.000070 cm^2/Vs The more negative zeta potential in the experimental group indicates greater colloidal stability of the AdMSC-derived sEV-enriched particles, suggesting that AdMSC-derived sEV-enriched particles from the experimental group are less prone to aggregation and therefore more stable in suspension compared to the control group (P≤0.05, Figure 14).

Assessing AdMSC-derived sEV-enriched particles for irritancy; irritant or non-irritant

In vivo irritation tests demonstrated that AdMSC-derived sEV-enriched particles from both the control and experimental groups were non-irritant in male New Zealand rabbits. No edema, erythema, or eschar formation was observed in any rabbit after administration of AdMSC-derived sEV-enriched particles (Table 2). The acceptable range in the irritation test was≤0.04, and all rabbits in the control and experimental groups scored zero, which is well within the acceptable range and indicates no adverse reactions (P>0.05, Table 2). Furthermore, comparing rabbits' body temperature changes before and after injection across groups showed a maximum deviation of 0.6 °C, underscoring the lack of systemic inflammatory response.

Consequently, the injected AdMSC-derived sEV-

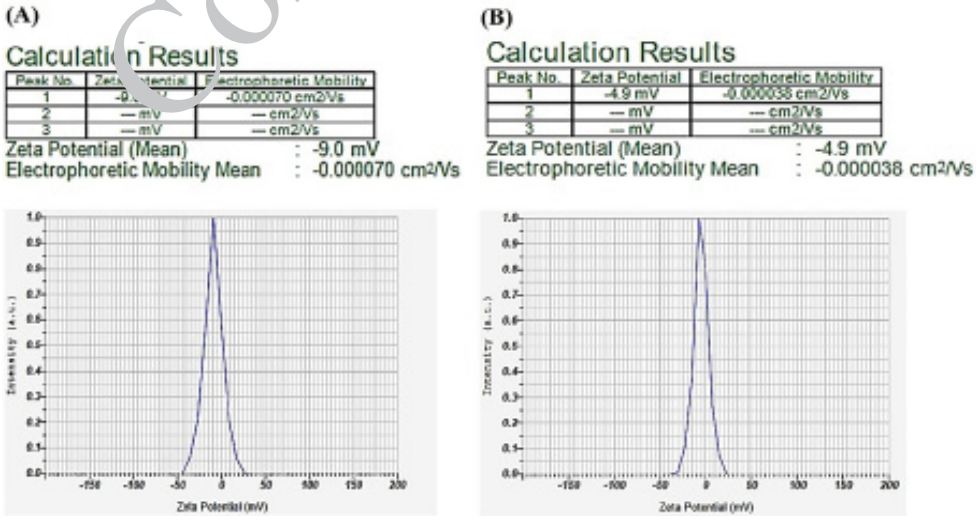


Figure 14. Surface charge, electrophoretic mobility, and colloidal stability of AdMSCs-derived sEVs-enriched particles in the experimental (A) and control (B) groups
AdMSCs: adipose-derived mesenchymal stem cells; sEVs: small extracellular vesicle

Corrected Proof

Table 2. *In vivo* irritation results of adipose-derived mesenchymal stem cells (AdMSC)-derived sEV-enriched particles between the control and experimental groups in male New Zealand rabbits

Groups		Acceptance indices	Score									Final Results irritant /Non-irritant
			Edema/hours			Erythema/hours			Eschar formation/hours			
			24±2	48±2	72±2	24±2	48±2	72±2	24±2	48±2	72±2	
MSC-derived particles from the control group	in nonpolar solvent	≤1	0	0	0	0	0	0	0	0	0	PASS
	in polar solution	≤1	0	0	0	0	0	0	0	0	0	
MSC-derived particles from the experimental group	in nonpolar solution	≤1	0	0	0	0	0	0	0	0	0	PASS
	in polar solvent	≤1	0	0	0	0	0	0	0	0	0	
Polar solutions		≤1	0	0	0	0	0	0	0	0	0	PASS
Non-polar solutions		≤1										PASS

enriched particles in all groups were classified as non-irritant based on these safety criteria (P>0.05, Table 3).

Evaluating AdMSC-derived sEV-enriched particles sensitization: Sensitizer or non-sensitizer

According to the Magnusson and Kligman grading system, intradermal injection of AdMSC-derived sEV-enriched particles did not result in observable edema (swelling), pruritus (itching), or erythema (redness) (Table 4). No significant differences in skin reactions were detected in albino guinea pigs between the control and experimental groups after 3 weeks (P>0.05). Furthermore, sensitization analysis indicated that AdMSC-derived sEV-enriched particles did not elicit local or systemic reactions in either group, including respiratory distress (wheezing, dyspnea), lethargy/malaise, and changes in appetite or behavior (Table 4, P>0.05).

Ensuring microbiological safety and sterility of AdMSC-derived sEV-enriched particles

The bioburden evaluation of AdMSC-derived sEV-enriched particles from both the control and experimental groups showed no microbial contamination (safety and sterility verification). The two groups showed no significant differences in microbial quality or sterility (P>0.05).

Both TAMC and TYMC remained within acceptable USP limits, with no microbial growth detected on SCDA or SDA plates. Additionally, cultures on EMB, BA, and Chocolate Agar confirmed the absence of Gram-positive and Gram-negative bacteria, including *Escherichia coli*, *Staphylococcus aureus*, and *Candida* species.

These findings confirm that AdMSC-derived sEV-enriched particles from both groups met microbiological acceptance criteria, demonstrating their sterility and suitability for further application (Table 5).

Assessing acute systemic toxicity of AdMSC-derived sEV-enriched particles: Toxic or non-toxic

Table 3. Body temperature measurements in male New Zealand rabbits before and at 30, 60, 90, 120, 150, and 180 minutes after administration of AdMSC-derived sEV-enriched particles in the control and experimental groups

Groups	Temperature before injection (°C)	Temperature after injection (°C) / Time (min)						
		30	60	90	120	150	180	Temperature difference
Control	40±0.2	40.2±0.1	40.3±0.3	40.4±0.2	40.4±0.2	40.5±0.3	40.5±0.2	<0.6 (PASS)
Experimental	40±0.3	40.3±0.2	40.3±0.2	40.4±0.2	40.4±0.4	40.5±0.3	40.5±0.4	<0.6 °C (PASS)

Table 4. Sensitization analyses of adipose-derived mesenchymal stem cells (AdMSC)-derived sEV-enriched particles from the control and experimental groups in the guinea pigs

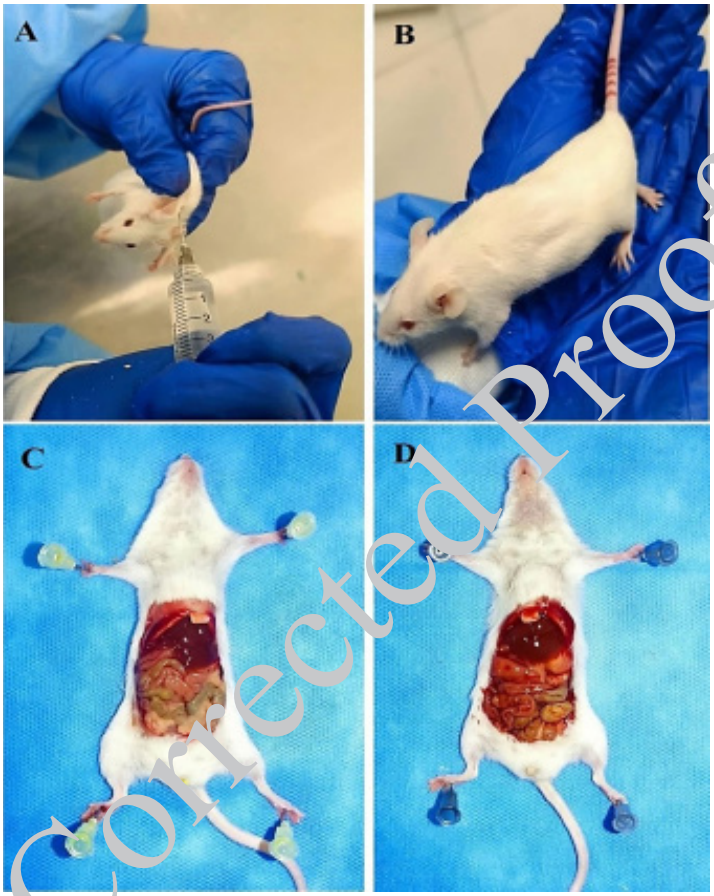
Groups	Local and systemic sensitization scores			Results
	24±2 hr	48±2 hr	72±2 hr	
Control	0	0	0	No detectable changes; PASS
Experimental	0	0	0	No visible changes; PASS

Corrected Proof

Table 5. Microbiological contamination of adipose-derived mesenchymal stem cells (AdMSC)-derived sEV-enriched particles under various culture conditions

Groups	Average TAMC (CFU/g)	Average TYMC (CFU/g)	Escherichia coli	Staphylococcus aureus	Pseudomonas aeruginosa	Candida
Control	10	<10	No	No	No	No
Experimental	10	<10	No	No	No	No

TAMC: total aerobic microbial count; TYMC: total yeast and mold count; CFU/g: colony-forming units per gram; AdMSC: adipose-derived mesenchymal stromal cell; sEV: small extracellular vesicle



Corrected Proof

Figure 15. Systemic toxicity assessment of AdMSCs-derived sEVs-enriched particles in NMRI mice. Mice received a single subcutaneous injection of sEVs-enriched particles at a dose of 0.5 mL/kg (A, B). Clinical signs and general condition of mice following administration of sEVs-enriched particles from the control (C) and experimental (D) groups

Table 6. Body weights of male and female naval medical research institute (NMRI) mice before and after injection of adipose-derived mesenchymal stem cells (AdMSC)-derived small extracellular vesicle (sEV)-enriched particles

Gender	Initial weights	Description	Groups / Body weights	
			Control	Experimental
Male	25-30 g	Start (Day 0)	28.7.8±1.5 g	27.3±1.8 g
		Day 7	29.6±1.1 g	28.6±1.9 g
		Day 14	30.1±1.8 g	29.4±1.8 g
		Day 21	30.6±1.2 g	29.8±1.3 g
		End (Day 28)	30.7±1.6 g	30.5±1.4 g
Female	25-30 g	Start of Test	27.6±1.3 g	26.9±1.5 g
		Day 7	28.2±1.3 g	27.2±1.4 g
		Day 14	27.8±1.9 g	28.5±1.5 g
		Day 21	28.9±0.8 g	28.9±1.7 g
		End (Day 28)	29.7 ±1.6 g	29.3±1.9 g

Table 7. Clinical observations of male and female NMRI mice before and after administration of adipose-derived mesenchymal stromal cell (AdMSC)-derived sEV-enriched particles in the control and experimental groups

Clinical signs	Female				Males			
	Before injection		After injection		Before injection		After injection	
	Control	Experimental	Control	Experimental	Control	Experimental	Control	Experimental
Respiratory	No	No	No	No	No	No	No	No
Locomotor activity	No	No	No	No	No	No	No	No
Skin: necrosis, fibrosis	No	No	No	No	No	No	No	No
Analgesic	No	No	No	No	No	No	No	No
Ocular and mucosal	No	No	No	No	No	No	No	No
Cardiovascular	No	No	No	No	No	No	No	No
Gastrointestinal	No	No	No	No	No	No	No	No
Death	No	No	No	No	No	No	No	No

sEV: small extracellular vesicle; NMRI: naval medical research institute

Figure 15 and Tables 6 and 7 present body weights and clinical signs in NMRI mice before and after administration of AdMSC-derived sEV-enriched particles. Subcutaneous administration of AdMSC-derived sEV-enriched particles at 50 ml/kg in mice showed no evidence of systemic toxicity, and all animals survived throughout the study. Generally, the absence of mortality, treatment-related clinical abnormalities, and significant changes in body weight confirmed that AdMSC-derived sEV-enriched particles in the control and experimental groups did not induce subacute systemic toxicity. Because no clinical signs of toxicity were observed, histopathological and clinical pathology assessments were not required in accordance with ISO 10993-11 and ISO 10993-12 guidelines.

Discussion

In the present study, a controlled stepwise serum deprivation (10% → 5% → 1% over 36 hr) was employed to induce a mild transient cellular stress response while preserving AdMSC viability, stemness potential, and metabolic activity. This approach allows for gradual cellular adaptation and reduces the likelihood of excessive cellular stress responses, including cell cycle arrest, metabolic suppression, or apoptosis associated with abrupt serum withdrawal during sEV production. We demonstrated that this controlled approach preserved the morphological and biological characteristics of AdMSCs and was associated with improved physicochemical properties of AdMSC-derived sEV-enriched particles without detectable cytotoxic effects. Compared with the control condition, low-serum culture maintained AdMSC viability (99%) and enhanced cell migration (>94% closure). It produced AdMSC-derived sEV-enriched particles with a more uniform particle size distribution (47±15 to 49±13 nm), altered surface charge characteristics, increased protein recovery (4.34 mg/ml), and acceptable preclinical biocompatibility. Collectively, these findings suggest that controlled serum reduction may serve as a practical upstream conditioning strategy to modulate the physicochemical properties of MSC-derived extracellular particle preparations while maintaining cellular safety (21, 31, 32). A fundamental prerequisite for interpreting extracellular vesicle-related studies is the confirmation that the parental cell population maintains its identity and functional characteristics throughout the experimental process. In the present study, AdMSCs maintained their characteristic spindle-shaped fibroblast-like morphology, high viability, multilineage differentiation capacity, and expression of canonical MSC-associated markers, including CD105, CD90, and CD29, with negligible expression of hematopoietic markers. These findings indicate that the observed alterations in extracellular particle characteristics were associated with controlled serum modulation rather than deterioration of the parental MSC population or loss of cellular identity. Consistent with the minimal criteria established by the International Society for Cell and Gene Therapy (ISCT), these results confirm that a stable and well-characterized MSC population was used for extracellular particle production (27, 28). No significant changes in AdMSC viability and apoptosis after sequential serum reduction are an important observation because excessive nutrient deprivation may induce irreversible cellular stress responses, including apoptosis, senescence, and the release of apoptotic bodies that can interfere with extracellular vesicle preparation and interpretation. Previous studies have demonstrated that the cellular response to nutrient limitation depends strongly on the duration and severity of stress exposure, with short-term controlled deprivation potentially inducing adaptive responses rather than cellular damage (29). Although the present study did not directly investigate intracellular signaling pathways, controlled serum reduction may influence nutrient-sensing and stress-adaptation mechanisms, including autophagy regulation, AMPK activation, mTOR signaling modulation, metabolic remodeling, and endosomal trafficking pathways involved in extracellular vesicle biogenesis. These mechanisms may explain the observed effects and warrant future validation through molecular analyses of markers such as LC3-II, Beclin-1, Rab27a, Alix, TSG101, and nSMase2 (30).

Another key finding of the present study was enhanced AdMSC migratory capacity after controlled serum reduction. MSC migration is a critical biological property associated with tissue recruitment, extracellular matrix remodeling, and regenerative responses. The increased scratch closure observed under low-serum conditions may represent an adaptive cellular response to altered nutrient availability, leading to changes in cytoskeletal organization, focal adhesion dynamics, and autocrine/paracrine signaling. Previous studies suggest that environmental modulation can regulate MSC migration through pathways associated with actin remodeling and growth factor responsiveness. In

Corrected Proof

particular, signaling networks involving RhoA/ROCK, PI3K/AKT, and MAPK/ERK have been implicated in MSC motility regulation; however, the current study did not experimentally assess these pathways and therefore interprets them as possible mechanisms rather than confirmed molecular explanations (33, 34). Structural characterization of AdMSC-derived sEV-enriched particles showed that controlled serum reduction markedly influenced particle distribution and morphology. Compared with the heterogeneous, polydisperse profile observed in the control condition, serum-reduced cultures generated particles with a narrower, more uniform distribution. This observation suggests that nutrient modulation may affect intracellular pathways regulating membrane remodeling, multivesicular body formation, and extracellular particle secretion. Previous studies show that cellular stress can modify extracellular vesicle characteristics by altering endosomal trafficking and membrane dynamics; however, the magnitude and direction of these effects depend heavily on cell origin and the applied stress protocol (22, 35). Haraszti *et al.* demonstrated that serum deprivation produces distinct extracellular vesicle responses among MSC sources, including adipose tissue-derived MSCs, bone marrow-derived MSCs, and umbilical cord-derived MSCs. Their findings emphasized that EV yield, composition, and biological properties are strongly influenced by cellular origin and experimental conditions. Importantly, differences in tissue origin may influence MSC metabolic responses and extracellular vesicle characteristics. AdMSCs possess distinct metabolic profiles, secretory patterns, and stress-adaptation capacities compared with BM-MSCs; therefore, variations observed between studies may reflect not only differences in serum conditions but also intrinsic biological differences among MSC sources (24, 36). Therefore, results from complete serum starvation protocols or other MSC sources cannot be directly extrapolated to the present study, in which AdMSCs were exposed to a gradual reduction in exosome-depleted FBS (10% → 5% → 1%) rather than abrupt serum withdrawal. This sequential adaptation strategy may explain preserved cellular viability and the observed improvement in particle homogeneity (22, 35).

The difference between FESEM and DLS measurements should also be carefully considered when interpreting particle size alterations. FESEM provides information regarding the dry-state diameter of fixed and dehydrated particles. In contrast, DLS measures hydrodynamic diameter in suspension, which is influenced by hydration layers, surface molecules, and particle interactions within the aqueous environment. Consequently, differences between FESEM-derived and DLS-derived sizes are expected and reflect methodological variation rather than inconsistency. Furthermore, the dominant DLS population around 34.1 nm requires cautious interpretation. Although this size range may represent a small extracellular vesicle subpopulation, previous studies have described non-vesicular nanoparticles, including exosome-like structures, with similar dimensions. Therefore, additional molecular characterization is required to distinguish authentic EV populations from other extracellular nanoparticles (37). This consideration is particularly important because particle size alone cannot confirm vesicular identity. Recent EV studies have emphasized that nanoscale extracellular particles may include heterogeneous populations with overlapping size ranges, including small EVs, exosome-like nanoparticles, and other non-vesicular structures. Therefore, integration of morphological analysis with molecular marker profiling is necessary for accurate classification (32, 37, 38).

The surface charge characteristics further supported the influence of controlled serum reduction on extracellular particle properties. The experimental group showed a more negative zeta potential than the control group, suggesting altered electrostatic interactions among particles. A more negative surface charge may increase electrostatic repulsion between particles and reduce aggregation tendency, thereby improving colloidal stability and potentially enhancing reproducibility during storage and formulation processes. However, although zeta potential is an important physicochemical parameter, it alone cannot determine the long-term stability or biological behavior of extracellular particle preparations, and additional stability studies under different storage conditions are required. These findings are consistent with previous nanomedicine studies demonstrating that surface charge modification can influence nanoparticle dispersion behavior and aggregation characteristics (39, 40).

Another important observation was the nearly twofold increase in total protein concentration in the serum-reduction group compared with the control group (4.34 mg/ml vs 2.17 mg/ml). The observed protein recovery falls within the range reported for MSC-derived extracellular vesicle preparations. However, direct comparison between studies remains challenging because of differences in cell source, culture conditions, isolation methods, and quantification approaches. Haraszti *et al.* similarly demonstrated that serum deprivation can alter the protein composition of MSC-derived exosomes, supporting the concept that nutrient modulation may influence extracellular particle cargo characteristics (24). This increase may indicate alterations in the biochemical composition or recovery efficiency of extracellular particle preparations following controlled nutrient modulation. However, total protein concentration should not be interpreted as a direct indicator of EV purity, cargo enrichment, or biological potency because protein measurements represent the overall protein content of the isolated preparation. Previous studies have demonstrated that cellular stress conditions can modify EV-associated protein profiles and molecular cargo; therefore, comprehensive proteomic analysis and cargo characterization, including miRNA profiling, are required to determine whether serum reduction selectively influences functional molecular components of AdMSC-derived extracellular particles (36, 41).

Using exosome-depleted FBS in both control and experimental groups is an important methodological strength of the present study. Because bovine-derived extracellular vesicles and serum proteins can interfere with EV isolation and characterization, exosome-depleted serum reduced the likelihood that observed differences resulted from external vesicle contamination rather than cellular responses. Nevertheless, without molecular purity assessment, complete exclusion of co-isolated non-EV components cannot be confirmed. Current extracellular vesicle characterization recommendations, including the MISEV2018 and MISEV2023 guidelines, require integrating multiple complementary approaches, including assessment of particle morphology, physicochemical properties, EV-associated markers, and potential contaminants. (32, 38) In particular, evaluating membrane-associated markers such as CD9, CD63, and CD81; intracellular vesicle-associated proteins such as Alix and TSG101; and appropriate non-EV markers can provide stronger evidence of EV identity and preparation purity. Since these molecular analyses were beyond the scope of the present investigation, the isolated preparations are referred to as "AdMSC-derived sEV-enriched particles" rather than definitively authenticated

Corrected Proof

small extracellular vesicles.

A major strength of this study was the comprehensive assessment of preclinical biocompatibility. Both control and serum-reduced AdMSC-derived sEV-enriched particle preparations demonstrated acceptable safety characteristics, including no microbial contamination, no cytotoxic effects, no detectable irritation or sensitization responses, and no acute systemic toxicity. These findings provide supportive evidence regarding the preclinical safety profile of the evaluated extracellular particle preparations; however, safety evaluation alone does not establish therapeutic efficacy. Functional studies investigating angiogenic activity, immunomodulatory effects, wound-healing capacity, or tissue-regeneration potential are required to determine whether the observed physicochemical modifications translate into improved biological outcomes. Therefore, although improved physicochemical properties may indicate better preparation quality, these parameters cannot replace biological potency assays. Future studies should evaluate whether serum reduction-induced changes affect recipient cell responses and therapeutic mechanisms (13, 18, 19).

From a translational perspective, establishing reproducible scalable manufacturing strategies remains a major challenge in developing MSC-derived extracellular vesicle-based products. Previous studies have emphasized that upstream manufacturing parameters, including nutrient availability, culture environment, and cellular stress conditions, can substantially influence EV quality attributes (42, 43). Colao *et al.* also highlighted the importance of controlling upstream manufacturing parameters, emphasizing that reproducible exosome production requires optimizing culture conditions, isolation strategies, and quality attributes to support future translational applications (44). More recently, Karimi *et al.* reported that serum deprivation, alone and in combination with hypoxia, altered the size distribution, surface charge, biochemical composition, and functional activity of AdMSC-derived exosome preparations, further supporting the sensitivity of extracellular vesicle characteristics to upstream conditioning strategies (45).

These findings suggest that controlled serum reduction may be a simple, potentially scalable upstream conditioning strategy to modulate extracellular particle characteristics while maintaining an acceptable safety profile. Nevertheless, additional investigations involving functional assays, standardized potency measurements, and disease-relevant In vivo models are required before therapeutic applications can be considered. Recent evidence reviewing adipose-derived MSC acellular products has likewise highlighted product heterogeneity, incomplete standardization of isolation and characterization methods, and regulatory challenges as important barriers to clinical translation (46). Accordingly, the current preparations should be considered research-grade or preclinical-grade extracellular particle products rather than clinical-grade materials until GMP-compliant manufacturing, sterility validation, and standardized potency assays are established (44). Despite these findings, several limitations remain. First, although the isolated particles exhibited morphological and physicochemical features consistent with sEV-enriched preparations, the lack of molecular EV marker characterization remains a key limitation. Future studies should incorporate EV-associated markers, including CD9, CD63, CD81, Alix, and TSG101, together with appropriate contamination markers, to improve authentication and purity assessment. Second, the present study did not evaluate inter-donor variability. Because MSC biological responses and EV characteristics can vary with donor-specific factors, future studies with larger donor cohorts are needed to assess the reproducibility of the observed effects. Third, extracellular particles were isolated using a single ultracentrifugation-based method; therefore, comparison with alternative isolation approaches, such as size-exclusion chromatography or combined purification strategies, may provide additional information regarding yield, purity, and reproducibility. Fourth, the absence of comprehensive cargo profiling represents another limitation. Although protein recovery increased, the functional significance of these biochemical changes remains unclear without proteomic, lipidomic, and RNA-based analyses. Finally, apoptosis assessment was performed using Acridine Orange staining, which provides mainly morphological and semi-quantitative information. Future investigations should incorporate more quantitative approaches, such as Annexin V/propidium iodide flow cytometry, to more accurately distinguish viable, apoptotic, and necrotic cell populations.

Conclusion

Controlled sequential reduction of exosome-depleted FBS from 10% to 5% and subsequently to 1% influenced selected biological characteristics of AdMSCs and modified the physicochemical characteristics of their sEV-enriched particle preparations without causing marked adverse effects under the condition evaluated in this study. Sequential serum reduction maintained cell viability comparable to the control condition and preserved multilineage differentiation potential. This strategy was also associated with altered cell migration behavior compared with the control condition. The resulting sEV-enriched particle preparations showed a shift toward a smaller, narrower particle-size distribution, a more negative zeta potential, and altered protein content. In addition, the evaluated safety assays showed no overt toxicity-related effects, irritation, sensitization, or microbial contamination. These findings suggest that controlled sequential serum reduction may represent a practical upstream culture strategy for modulating the physicochemical profile of AdMSC-derived sEV-enriched particle preparations. However, the present study does not establish increased EV yield, definitive EV identity or purity, or enhanced therapeutic efficacy. Further investigations incorporating molecular EV marker characterization, cargo profiling, and functional assays are warranted.

Acknowledgment

The authors gratefully acknowledge the medical and administrative staff of Gandhi Hospital (Tehran, Iran) for their invaluable assistance and coordination during sample collection.

Ethics Approval and Consent to Participate

The Research Ethics Committee of Islamic Azad University, Science and Research Branch, Tehran, Iran, approved the study protocol (Approval ID: IR.IAU.SRB.REC.1403.018). All procedures involving human participants were conducted in strict accordance with the ethical standards of the institutional research committee and the 1964 Declaration of Helsinki and its later amendments. Written informed consent was obtained from all individual participants (5 healthy donors) before adipose tissue collection.

Availability of Data and Materials

The datasets generated and/or analyzed during the current study are available from the corresponding author

Corrected Proof

Funding

This research received no specific financial support from public, commercial, or not-for-profit funding agencies. The student (Pegah Rajabi) and the corresponding author covered the research costs.

Authors' Contributions

P R and N A contributed equally to the conceptualization, methodology, investigation, and writing of the original draft. H J contributed to the methodology and investigation. B H was responsible for supervision, project administration, and writing review and editing. All authors have read and approved the final version of the manuscript.

Conflicts of Interest

The authors declare no competing interests.

Declaration

The authors declare that they have not used AI-generated work in this manuscript.

References

1. Till JE, McCulloch EA. A direct measurement of the radiation sensitivity of normal mouse bone marrow cells. Radiat Res 1961; 14: 213-222.
2. Friedenstein AJ, Petrakova KV, Kurolesova AI, Frolova GP. Heterotopic of bone marrow. Analysis of precursor cells for osteogenic and hematopoietic tissues. Transplantation 1968; 6: 230-247.
3. Lee DE, Ayoub N, Agrawal DK. Mesenchymal stem cells and cutaneous wound healing: Novel methods to increase cell delivery and therapeutic efficacy. Stem Cell Res Ther 2016; 7: 37.
4. Spees JL, Lee RH, Gregory CA. Mechanisms of mesenchymal stem/stromal cell function. Stem Cell Res Ther 2016; 7: 12
5. Vizoso FJ, Eiro N, Cid S, Schneider J, Perez-Fernandez R. Mesenchymal stem cell secretome: Toward cell-free therapeutic strategies in regenerative medicine. Int J Mol Sci 2017; 18: 1852.
6. Zhang J, Guan J, Niu X, Hu G, Guo S, Li Q, *et al.* Exosomes released from human induced pluripotent stem cells-derived MSCs facilitate cutaneous wound healing by promoting collagen synthesis and angiogenesis. J Transl Med 2015; 13: 49.
1. Till JE, McCulloch EA. A direct measurement of the radiation sensitivity of normal mouse bone marrow cells. Radiat Res 1961; 14: 213-222.
2. Friedenstein AJ, Petrakova KV, Kurolesova AI, Frolova GP. Heterotopic of bone marrow. Analysis of precursor cells for osteogenic and hematopoietic tissues. Transplantation 1968; 6: 230-247.
3. Lee DE, Ayoub N, Agrawal DK. Mesenchymal stem cells and cutaneous wound healing: Novel methods to increase cell delivery and therapeutic efficacy. Stem Cell Res Ther 2016; 7: 37.
4. Spees JL, Lee RH, Gregory CA. Mechanisms of mesenchymal stem/stromal cell function. Stem Cell Res Ther 2016; 7: 125.
5. Vizoso FJ, Eiro N, Cid S, Schneider J, Perez-Fernandez R. Mesenchymal stem cell secretome: Toward cell-free therapeutic strategies in regenerative medicine. Int J Mol Sci 2017; 18: 1852.
6. Zhang J, Guan J, Niu X, Hu G, Guo S, Li Q, *et al.* Exosomes released from human induced pluripotent stem cells-derived MSCs facilitate cutaneous wound healing by promoting collagen synthesis and angiogenesis. J Transl Med 2015; 13: 49.
7. Goodarzi P, Larijani B, Alavi-Moghadam S, Tayanloo-Beik A, Mohamadi-Jahani F, Ranjbaran N, *et al.* Mesenchymal stem cells-derived exosomes for wound regeneration. Adv Exp Med Biol 2018; 1119: 119-131.
8. Poltavtseva RA, Poltavtsev AV, Lutsenko GV, Svirshchevskaya EV. Myths, reality and future of mesenchymal stem cell therapy. Cell Tissue Res 2019; 375: 563-574.
9. Lopez-Verrilli MA, Caviedes A, Cabrera A, Sandoval S, Wyneken U, Khoury M. Mesenchymal stem cell-derived exosomes from different sources selectively promote neuritic outgrowth. Neuroscience 2016; 320: 129-139.
10. Nazari D, Heidari B, Akbari N, Soleymani Z. Principles and regulatory pathways of exosome-based products in wound healing: Insights from the Iranian Food and Drug Administration guideline. Iran J Basic Med Sci 2026; 29: 1337-1354.
11. Thirabanjasak D, Tantiwongse K, Thorner PS. Angiomyeloproliferative lesions following autologous stem cell therapy. J Am Soc Nephrol 2010; 21: 1218-1222.
12. Yang C, Luo L, Bai X, Shen K, Liu K, Wang J, *et al.* Highly-expressed micoRNA-21 in adipose derived stem cell exosomes can enhance the migration and proliferation of the HaCaT cells by increasing the MMP-9 expression through the PI3K/AKT pathway. Arch Biochem Biophys 2020; 681: 108259.
13. Chen B, Li Q, Zhao B, Wang Y. Stem cell-derived extracellular vesicles as a novel potential therapeutic tool for tissue repair. Stem Cells Transl Med 2017; 6: 1753-1758.
14. Meiliana A, Dewi NM, Wijaya A. Mesenchymal stem cell secretome: Cell-free therapeutic strategy in regenerative medicine. Indones Biomed J 2019; 11: 113-124.
15. Duscher D, Barrera J, Wong VW, Maan ZN, Whittam AJ, Januszyk M, *et al.* Stem cells in wound healing: The future of regenerative medicine? A mini-review. Gerontology 2016; 62: 216-225.
16. Perez-Hernandez J, Redon J, Cortes R. Extracellular vesicles as therapeutic agents in systemic lupus erythematosus. Int J Mol Sci 2017; 18: 71
17. Bai L, Shao H, Wang H, Zhang Z, Su C, Dong L, *et al.* Effects of mesenchymal stem cell-derived exosomes on experimental autoimmune uveitis. Sci Rep 2017; 7: 4323.
18. Mitchell R, Mellows B, Sheard J, Antonioli M, Kretz O, Chambers D, *et al.* Secretome of adipose-derived mesenchymal stem cells promotes skeletal muscle regeneration through synergistic action of extracellular vesicle cargo and soluble proteins. Stem Cell Res Ther 2019; 10: 116.
19. Kumar LP, Kandoi S, Misra R, Vijayalakshmi S, Rajagopal K, Verma RS. The mesenchymal stem cell secretome: A new paradigm towards cell-free therapeutic mode in regenerative medicine. Cytokine Growth Factor Rev 2019; 46: 1-9.
20. Sun T, Li M, Liu Q, Yu A, Cheng K, Ma J, *et al.* Insights into optimizing exosome therapies for acute skin wound healing and other tissue repair. Front Med 2024; 18: 258-284.
21. Sarvari A, Niasari-Naslaji A, Shirazi A, Heidari B, Borjian Boroujeni S, Moradi MH, *et al.* Effect of intra-ovarian injection of mesenchymal stem cells or its conditioned media on repeated OPU-IVEP outcomes in Jersey heifers and its relationship with follicular fluid inflammatory markers. Avicenna J Med Biotechnol 2024; 16: 16-28.
22. Jung PY, Ryu H, Rhee KJ, Hwang S, Lee CG, Gwon SY, *et al.* Adipose tissue-derived mesenchymal stem cells cultured at high density express IFN-β and TRAIL and suppress the growth of H460 human lung cancer cells. Cancer Lett 2019; 440-441: 202-210.
23. Vu BT, Le HT, Nguyen KN, Pham PV. Hypoxia, serum starvation, and TNF-α can modify the immunomodulation potency of human adipose-derived stem cells. Adv Exp Med Biol 2021; doi: 10.1007/5584_2021_672.
24. Haraszti RA, Miller R, Dubuke ML, Rockwell HE, Coles AH, Sapp E, *et al.* Serum deprivation of mesenchymal stem cells improves exosome activity and alters lipid and protein composition. iScience 2019; 16: 230-241.
25. Oskowitz A, McFerrin H, Gutschow M, Carter ML, Pochampally R. Serum-deprived human multipotent mesenchymal stromal cells are highly angiogenic. Stem Cell Res 2011; 6: 215-225.
26. Bakopoulou A, Kritis A, Andreadis D, Papachristou E, Leyhausen G, Koidis P, *et al.* Angiogenic potential and secretome of human apical papilla mesenchymal stem cells in various stress microenvironments. Stem Cells Dev 2015; 24: 2496-2512.

Corrected Proof

27. Hu C, Li L. Preconditioning influences mesenchymal stem cell properties *in vitro* and *in vivo*. J Cell Mol Med 2018; 22: 1428-1442.
28. Heidari B, Shirazi A, Akhondi MM, Hassanpour H, Behzadi B, Naderi MM, *et al*. Comparison of proliferative and multilineage differentiation potential of sheep mesenchymal stem cells derived from bone marrow, liver, and adipose tissue. Avicenna J Med Biotechnol 2013; 5: 104-117.
29. Karimi M, Heidari B, Jafary H, Zandsalimi K. The quality and quantity of nanoparticles extracted from human adipose tissue-derived mesenchymal stem cells. Avicenna J Med Biotechnol 2025; 17: 186-195.
30. Kholgh H, Eshghabadi F, Jafary H, Zandsalimi K, Akbari N, Soltani A, *et al*. Characterization of exosomes from hypoxia-activated human amniotic membrane mesenchymal stem cells. Iran J Basic Med Sci 2026; 29: 544-577.
31. Bari E, Ferrarotti I, Di Silvestre D, Grisoli P, Barzon V, Balderacchi A, *et al*. Adipose mesenchymal extracellular vesicles as alpha-1-antitrypsin physiological delivery systems for lung regeneration. Cells 2019; 8: 965.
32. Welsh JA, Goberdhan DCI, O'Driscoll L, Buzas EI, Blenkiron C, Bussolati B, *et al*. Minimal information for studies of extracellular vesicles (MISEV2023): From basic to advanced approaches. J Extracell Vesicles 2024; 13: e12404.
33. Hou M, Ji L, Li D, Xiao Q, Hu X. Serum starvation-induced cholesterol reduction increases melanoma cell susceptibility to cytotoxic T lymphocyte killing. Sci Rep 2025; 15: 18364.
34. Shi H, Inankur B, Yin J. Serum starvation impacts rhinovirus spread from cell to cell. Virology 2025; 604: 110408.
35. Wang Y, Gao J, Fan B, Hu Y, Yang Y, Wu Y, *et al*. Effects of long-term serum starvation on autophagy, metabolism, and differentiation of porcine skeletal muscle satellite cells. Vet Sci 2025; 12: 11.
36. Giannasi C, Niada S, Della Morte E, Casati SR, De Palma C, Brini AT. Serum starvation affects mitochondrial metabolism of adipose-derived stem/stromal cells. Cytotherapy 2023; 25: 704-71[illegible]
37. Rajab Zadeh H, Heidari B, Jafary H, Zandsalimi K, Akbari N. Comprehensive characterization of human placental extract-derived nanovesicles: Insight into structural, morphological, chemical, biological, and biocompatible properties. BioNanoScience 2026; 16: 169.
38. Théry C, Witwer KW, Aikawa E, Alcaraz MJ, Anderson JD, Andriantsitohaina R, *et al*. Minimal information for studies of extracellular vesicles 2018 (MISEV2018): A position statement of the International Society for Extracellular Vesicles and update of the MISEV2014 guidelines. J Extracell Vesicles 2018; 7: 1535750.
39. Sahebi R, Akbari N, Bayat Z, Rashidmayvan M, Mansoori A, Beihaghi M. A summary of autophagy mechanisms in cancer cells. Res Biotechnol Environ Sci 2022; 1: 28-35.
40. Yang Q, Hu Y, Lv J, Xue J, Chen J, Wang C, *et al*. Serum starvation induces density-dependent apoptosis via HIF-1 activation and JNK suppression. Acta Biochim Biophys Sin (Shanghai) 2025; doi: 10.3724/abbs.2025161.
41. Nuschke A, Rodrigues M, Wells AW, Sylakowski K, Wells A. Mesenchymal stem cells/multipotent stromal cells are glycolytic and thus glucose is a limiting factor of *in vitro* models of MSC starvation. Stem Cell Res Ther 2016; 7: 179.
42. Johnstone BH, Gu D, Lin CH, Du J, Woods EJ. Identification of a fundamental cryoinjury mechanism in MSCs and its mitigation through cell-cycle synchronization prior to freezing. Cryobiology 2023; 113: 104592.
43. Kim JY, Rhim WK, Seo HJ, Lee JY, Park CG, Han DK. Comparative analysis of MSC-derived exosomes depending on cell culture media for regenerative bioactivity. Tissue Eng Regen Med 2021; 18: 355-367.
44. Colao IL, Corteling R, Bracewell D, Wall I. Manufacturing Exosomes: A Promising Therapeutic Platform. Trends Mol Med 2018; 24: 242-256.
45. Karimi M, Zandsalimi K, Jafary H, Akbari N, Heidari B. Comparative effects of hypoxia and serum deprivation on the morphological, structural, chemical, biological and functional characteristics of exosomes from adipose-derived mesenchymal stem cells. Research Square [Preprint]. 2025. doi: 10.21203/rs.3.rs-7136519/v1.
46. Akbari N, Heidari B, Totonchi M. Adipose-derived mesenchymal stromal cells and their acellular derivatives in cutaneous wound healing and pathological scarring: A narrative review. Cell Tissue Bank 2026; 27: 35.

Corrected Proof